

Interpretation of AMS-02 electrons and positrons data

To cite this article: M. Di Mauro *et al* JCAP04(2014)006

View the [article online](#) for updates and enhancements.

Related content

- [Dark matter vs. astrophysics in the interpretation of AMS-02 electron and positron data](#)
Mattia Di Mauro, Fiorenza Donato, Nicolao Fornengo *et al.*
- [AMS-02 in Space: Physics Results](#)
Nicola Tomassetti and AMS collaboration
- [Interpretation of AMS-02 results: correlations among dark matter signals](#)
Andrea De Simone, Antonio Riotto and Wei Xue

Recent citations

- [Review of the results of measurements of the fluxes of the charged components of galactic cosmic rays in the experiments PAMELA and AMS-02](#)
V. V. Alekseev *et al*
- [Pulsar Wind Nebulae with Bow Shocks: Non-thermal Radiation and Cosmic Ray Leptons](#)
A. M. Bykov *et al*
- [Secondary cosmic positrons in an inhomogeneous diffusion model](#)
Rolf Kappl and Annika Reinert

Interpretation of AMS-02 electrons and positrons data

M. Di Mauro,^{a,b,c} F. Donato,^{a,b} N. Fornengo,^{a,b} R. Lineros^d
and A. Vittino^{a,b,e}

^aDipartimento di Fisica, Università di Torino,
via P. Giuria 1, 10125 Torino, Italy

^bIstituto Nazionale di Fisica Nucleare, Sezione di Torino,
Via P. Giuria 1, 10125 Torino, Italy

^cLaboratoire d'Annecy-le-Vieux de Physique Théorique (LAPTh), Univ. de Savoie, CNRS,
B.P.110, Annecy-le-Vieux F-74941, France

^dAHEP Group, Institut de Física Corpuscular, C.S.I.C. Universitat de València,
Edificio Institutos de Paterna, Apt 22085, E-46071 Valencia, Spain

^eInstitut de Physique Théorique, CNRS,
URA 2306 & CEA/Saclay, F-91191 Gif-sur-Yvette, France

E-mail: mattia.dimauro@to.infn.it, donato@to.infn.it, fornengo@to.infn.it,
rlineros@ific.uv.es, vittino@to.infn.it

Received February 7, 2014

Accepted February 25, 2014

Published April 4, 2014

Abstract. We perform a combined analysis of the recent AMS-02 data on electrons, positrons, electrons plus positrons and positron fraction, in a self-consistent framework where we realize a theoretical modeling of all the astrophysical components that can contribute to the observed fluxes in the whole energy range. The primary electron contribution is modeled through the sum of an average flux from distant sources and the fluxes from the local supernova remnants in the Green catalog. The secondary electron and positron fluxes originate from interactions on the interstellar medium of primary cosmic rays, for which we derive a novel determination by using AMS-02 proton and helium data. Primary positrons and electrons from pulsar wind nebulae in the ATNF catalog are included and studied in terms of their most significant (while loosely known) properties and under different assumptions (average contribution from the whole catalog, single dominant pulsar, a few dominant pulsars). We obtain a remarkable agreement between our various modeling and the AMS-02 data for all types of analysis, demonstrating that the whole AMS-02 leptonic data admit a self-consistent interpretation in terms of astrophysical contributions.

Keywords: ultra high energy cosmic rays, particle acceleration, cosmic ray theory, cosmic ray experiments

ArXiv ePrint: [1402.0321](https://arxiv.org/abs/1402.0321)

Contents

1	Introduction	1
2	Sources of galactic positron and electrons	2
2.1	Primary electrons from SNR	2
2.2	Primary electrons and positrons from PWN	3
2.3	Secondary positron and electrons	5
3	The propagation of electrons and positrons in the Galaxy	6
4	Fit to AMS-02 data: method and free parameters	8
4.1	The case for secondary positrons	9
4.2	The case for pulsars cut-off energy	12
5	High-energy window and local sources	12
5.1	“Single-source” analysis	14
5.2	“Powerful-sources” analysis	15
6	Conclusions	19

1 Introduction

A huge experimental effort undertaken in the last decades has led to increasingly accurate measurements of cosmic rays (CRs) by means of space borne detectors. In particular, excellent data have been provided for the positron fraction ($e^+/(e^+ + e^-)$) and for the absolute positron (e^+), electron (e^-) and total ($e^+ + e^-$) CR spectra by the Pamela [1–3] and *Fermi-LAT* [4, 5] Collaborations. Very recently, also the AMS-02 Collaboration has provided its first data on the positron fraction spectrum measured by the Alpha Magnetic Spectrometer installed on the International Space Station [6], and preliminary results for the other leptonic observables [7, 8]. The data cover an energy range spanning from about one GeV up to hundreds of GeV, depending on the species.

The most direct interpretation of these data refers to secondary production from nuclear collisions with primary CRs and the atoms of the interstellar medium (ISM), as well as to galactic astrophysical sources injecting fresh primary leptons into the ISM (see e.g. ref. [9] and references therein, and refs. [10–22]). The observed raise of the positron fraction, firstly reported by the Pamela Collaboration and confirmed with higher precision by the AMS-02 data, has stimulated an extensive speculation on a possible dark matter (DM) contribution at high energies [23–40].

In this paper, we explore at which level the new AMS-02 data on the whole leptonic observables may be accommodated in a purely astrophysical (i.e. without invoking contributions from exotic sources such as DM annihilation) scenario, which counts the contribution from powerful stellar sources as well as from secondary reactions among primary CRs and atoms in the ISM. Specifically, we study the possible contribution that supernova remnants (SNRs) can give to high energy electron fluxes, and pulsar wind nebulae (PWN) to both positron and electron spectra. Whenever available, independent data on these sources are taken into

account as constraints on their emission properties. We also employ the new preliminary AMS-02 data for proton and helium cosmic fluxes, in order to obtain a new evaluation of the secondary e^+ and e^- fluxes. All these components are added together and propagated in the Milky Way. A key point of our analysis is the requirement for any theoretical model to fit *simultaneously* all the four AMS-02 leptonic observables, namely the $e^+/(e^+ + e^-)$, e^+ , e^- and $e^+ + e^-$ spectra. As we will show in next sections, we find several astrophysical models compatible with all the AMS-02 leptonic data. Our results imply that a consistent and global picture of the Galaxy is possible, at least for the leptonic sector. Even more so, we show that high precision, low energy positron data, such as the ones collected by AMS-02, are on the verge of acting as a remarkable tool to constrain propagation models, and cooperate with the boron-to-carbon observations to this fundamental task. Our analyses are all implemented by a thorough estimation of the underlying possible uncertainties. This method allows us to derive predictions on the AMS-02 data at very high energy, expected after some increase in the collected statistics. As a final remark, we notice that our analysis indicates that there is no particular need to invoke DM annihilation in the halo of the Milky Way in order to explain high energy positron and electron data.

2 Sources of galactic positron and electrons

As a first step of our analysis, we describe and model the various possible galactic sources for positrons and electrons. We can, as usual, identify two main categories: primary production, which refers to electrons and positrons directly injected in the galactic medium from astrophysical sources, like PWN and SNR; secondary production, which refers to electrons and positrons produced from a spallation reaction of a progenitor cosmic ray in the Galaxy.

2.1 Primary electrons from SNR

SNR in our Galaxy are believed to be the major accelerators of charged particles up to very high energies (at least 100 TeV), via a first-type Fermi mechanism [41–44]. Among accelerated species there are also electrons. The mechanism of acceleration of cosmic rays through non-relativistic expanding shock-waves, activated by the star explosion, predicts power-law spectra with a cut-off at high energies:

$$Q(E) = Q_0 \left(\frac{E}{E_0} \right)^{-\gamma} \exp \left(-\frac{E}{E_c} \right), \quad (2.1)$$

where Q_0 is the normalization of the spectrum, γ is the power-law index, E_c is the cut-off energy which in our analysis we fix at $E_c = 2$ TeV, and $E_0 = 1$ GeV is just a reference value. The values for the spectral index γ for electrons are typically found around 2 [41, 45], although they exhibit significant variations in analyses of radio data. Radio and gamma-ray observations also indicate that E_c might be in the TeV range (see e.g. ref. [46–50]). The value of Q_0 is by far non trivial to fix, but can in principle be estimated from radio data on single sources, assuming that the radio flux B_r^ν at a specific frequency ν is entirely due to synchrotron emission of the ambient electrons in the SNR magnetic field B [14, 51, 52]:

$$Q_0 = 1.2 \cdot 10^{47} \text{ GeV}^{-1} (0.79)^\gamma \left[\frac{d}{\text{kpc}} \right]^2 \left[\frac{\nu}{\text{GHz}} \right]^{(\gamma-1)/2} \left[\frac{B}{100 \mu\text{G}} \right]^{-(\gamma+1)/2} \left[\frac{B_r^\nu}{\text{Jy}} \right] \quad (2.2)$$

where d is the distance of the source from the observer. The well-known relation between the radio and electron flux index $\alpha_r = (\gamma - 1)/2$ is here manifest.

The most complete SNR catalog is provided by the Green catalog [53], where 274 SNRs are listed. Among them, 88 objects have a distance measurement, and 209 have an observed radio spectral index. Following the procedure described in ref. [14], we can determine the average values for the relevant parameters for those 88 SNRs with a clear distance information. We obtain: $\langle\alpha_r\rangle = 0.50 \pm 0.15$, $\langle d^2 B_r^{1\text{GHz}}\rangle = \exp(7.1 \pm 1.7)$ Jy kpc². From these results we then infer: $\langle\gamma\rangle = 2 \cdot \langle\alpha_r\rangle + 1 = 2.0 \pm 0.3$. Moreover, fixing a typical magnetic field of $B = 30 \mu\text{G}$ (adopted in the following of our analysis) [47, 52, 54–60], and employing eq. (2.2), we estimate $\langle Q_0\rangle = 9.0 \times 10^{49} \text{ GeV}^{-1}$ for an index $\gamma = 2$, which implies a total emitted energy of $\langle E_\star \cdot f \cdot \Gamma_\star\rangle = 8.9 \times 10^{50} \text{ GeV} = 1.4 \times 10^{48} \text{ erg}$ (for a cut-off energy $E_c = 2 \text{ TeV}$), where $\Gamma_\star \approx [2, 4]$ is the SN explosion rate [61, 62], E_\star is the kinetic energy released by the explosion, and $f \approx [10^{-5}, 10^{-4}]$ [42] is the fraction of this energy converted into electrons.

For the purposes of the analysis discussed in the next sections, we divide the SNR population into a *near* component, for sources lying at distances $d \leq 3$ kpc from the Earth, and a *far* component, for sources located outside this region. For a discussion on the choice of the separation distance between far and close sources, see ref. [14]. In the catalog we find 41 near-SNRs, out of which only 35 have a measured distance, age, radio flux and spectral index. Therefore only these 35 sources have been taken into consideration in our analysis. These sources are listed in table 1, where we report their characteristics: together with the Green-catalog name and (when available) the association name, we list the radio flux at 1 GHz $B_r^{1\text{GHz}}$, the radio index α_r , the distance d and the age T . As done in ref. [14] (note that the critical distance, which separates near from far SNR, is now assumed to be 3 kpc instead of 2 kpc), the near-SNRs are considered as single, independent sources, with their typical parameters fixed to the ones reported in table 1 or derived via eq. (2.2). The far-SNR population is instead treated as an average source population, with typical parameters (Q_0 and γ) fixed according to the analysis of section 4, and following the radial profile derived in ref. [63].

2.2 Primary electrons and positrons from PWN

Pulsars, rapidly spinning neutron stars with a strong surface magnetic field, are considered to be among the most powerful sources of electrons and positrons in the Galaxy [15, 153–157]. It is believed that the rotating magnetic field of the pulsar generates an intense electric field that can tear particles apart from the neutron star surface. These charged particles can then be accelerated and induce an electromagnetic cascade through the emission of curvature radiation that, in turns, produces again particle/antiparticle pairs [158–160]. The star, and the wind of charged particles that surrounds it, are initially located inside the remnants of the supernova explosion that creates the pulsar. The impact of the relativistic wind produced by the pulsar on the much slower ejecta of the supernova usually creates a reverse shock (the so-called *termination shock*) that propagates backwards, towards the pulsar [161]. In the region bound by the wind termination shock on one side and the ejecta on the other side, a bubble of relativistically hot magnetized plasma is created: this is the so-called pulsar wind nebula (PWN). The termination shock is also the place where the incoming pairs are accelerated to very high energies. After acceleration, these particles enter the PWN and then are trapped by the PWN magnetic field until it is disrupted. What is usually assumed is that the accelerated particles are completely released into the interstellar medium (ISM) after a time of about 50 kyr from the nebula formation. As stressed in ref. [162], since this injection is assumed to be quite fast and the subsequent energy emission of the pulsar negligible, a

Green	Association	$B_r^{1\text{GHz}}[\text{Jy}]$	α_r	d [kpc]	T [kyr]	Refs.
G006.4-00.1	W28	287 ± 27	-0.35	2.0 ± 0.4	[33,150]	[53, 64, 65]
G018.9-01.1		37 ± 2	-0.39 ± 0.03	2	[4.4,6.1]	[53, 66–69]
G034.7-00.4	W44	213 ± 11	-0.33 ± 0.05	3.0	[10,20]	[53, 66, 70–74]
G065.3+05.7		52 ± 2	-0.58 ± 0.07	0.9 ± 0.1	26	[53, 75–77]
G065.7+01.2	DA495	4.88 ± 0.25	-0.57 ± 0.01	[1.0,1.8]	20	[53, 66, 78, 79]
G069.0+02.7	CTB80	60 ± 10	-0.36 ± 0.02	2	20	[66, 80–83]
G074.0-08.5	Cygnus loop	175 ± 30	-0.40 ± 0.06	0.58 ± 0.06	10	[53, 84–86]
G078.2+02.1	DR4	275 ± 25	-0.75 ± 0.03	1.5 ± 0.1	7	[53, 87–89]
G082.2+05.3	W63	105 ± 10	-0.36 ± 0.08	[1.6,3.3]	[13,27]	[53, 81, 90, 91]
G089.0+04.7	HB21	200 ± 15	-0.27 ± 0.07	1.7 ± 0.5	5.6 ± 0.3	[53, 81, 92–94]
G093.3+06.9	DA530	7.0 ± 0.5	-0.45 ± 0.04	2.2 ± 0.5	[5.2,6.6]	[53, 81, 95, 96]
G093.7-00.2	DA551	42 ± 7	-0.52 ± 0.12	1.5 ± 0.2	[29,74]	[53, 81, 97, 98]
G109.1-01.0	CTB109	20.2 ± 1.1	-0.45 ± 0.04	3.0 ± 0.5	[13,17]	[53, 66, 81, 99–101]
G113.0+0.2		3.8 ± 1.0	-0.45 ± 0.25	3.1	20	[53, 66, 102]
G114.3+00.3		6.4 ± 1.4	-0.49 ± 0.25	0.7	7.7	[53, 60, 81, 103]
G116.5+01.1		10.9 ± 1.2	-0.16 ± 0.11	1.6	[15,50]	[53, 60, 81, 103]
G116.9+00.2	CTB 1	7.9 ± 1.3	-0.33 ± 0.13	1.6	[15,50]	[53, 60, 66, 81, 103]
G119.5+10.2	CTA 1	42 ± 3	-0.57 ± 0.06	1.4 ± 0.3	[5,15]	[53, 104, 105]
G127.1+00.5	R5	12 ± 1	-0.43 ± 0.10	1.0 ± 0.1	[20,30]	[53, 60, 81, 106, 107]
G130.7+03.1	3C58	35 ± 3	-0.07 ± 0.02	3.0 ± 0.2	[2.7,5.4]	[53, 66, 81, 108, 109]
G132.7+01.3	HB3	36 ± 3	-0.59 ± 0.14	2.2 ± 0.2	30	[53, 81, 94, 110, 111]
G156.2+05.7		5.0 ± 0.8	-0.53 ± 0.17	1.0 ± 0.3	[15,26]	[53, 81, 112–115]
G160.9+02.6	HB9	88 ± 9	-0.59 ± 0.02	0.8 ± 0.4	[4,7]	[53, 60, 81, 92, 116]
G180.0-01.7	S147	74 ± 12	-0.30 ± 0.15	$1.47_{-0.27}^{+0.42}$	[30,40]	[53, 92, 117–120]
G184.6-05.8	Crab	1040	-0.3	2.0 ± 0.5	[6,9]	[53, 121]
G189.1+03.0	IN 443	160 ± 5	-0.36 ± 0.04	1.5 ± 0.1	[20,30]	[53, 60, 92, 122, 123]
G205.5+00.5	Monoceros	156 ± 20	-0.47 ± 0.06	1.63 ± 0.25	[29,150]	[53, 124, 124–127]
G260.4-03.4	Puppis A	137 ± 10	-0.52 ± 0.03	2.2 ± 0.3	3.7	[53, 128–131]
G263.9-03.3	Vela(XYZ)	2000 ± 700	variable	$2.94_{-0.50}^{+0.76}$	11.3	[53, 53, 132–136]
G266.2-01.2	Vela Jr	± 4	-0.3	0.75	[1.7,4.3]	[53, 137–140]
G315.1+02.7		35 ± 6	-0.7	1.7	[40,60]	[53, 141, 142]
G315.4-02.3	RCW 86	49	-0.61	2.3 ± 0.2	10	[53, 55, 143–145]
G327.6+14.6	SN1006	16 ± 2	-0.6	2.2 ± 0.1	[0.9,1.3]	[53, 146–149]
G330.0+15.0	Lupus loop	350	-0.5	1.2 ± 0.4	[20,50]	[53, 150, 151]
G347.3005		4 ± 1	-0.3	1	[1.6,4.9]	[53, 59, 152]

Table 1. Characteristic parameters for our sample of near (≤ 3 kpc) SNRs: the columns report the Green-catalog name, the association name, the radio flux at 1 GHz $B_r^{1\text{GHz}}$, the radio index α_r , the distance d [kpc] and the SNR age T [kyr].

mature pulsar can be treated as a burst-like source of e^\pm . The emitted leptons can then reach the Earth with huge Lorentz factors (see, e.g., ref. [163] for the Crab Nebula).

In order to determine the flux of emitted electrons and positrons by a pulsar, we follow the model described in ref. [14] (and references therein) and remind here only the main ingredients relevant to our analysis. Nevertheless, we remark here that the actual process through which the electrons are injected from the PWN into the ISM is only very little known. As explained in ref. [164], the spectrum of electrons and positrons trapped inside the PWN can be inferred by observing their broadband emission which is due to synchrotron radiation (at low energies) and to inverse Compton (IC) scattering off background photons (at higher energies). This broadband spectrum shows a break between the radio and X-ray regimes which is believed to be the result of synchrotron cooling. However, even the time evolution of the electrons spectrum inside the PWN is not known: this means that the snapshot picture that one can derive from the observation of the broadband spectrum of the emitted radiation is not necessarily representative of the electron spectrum that eventually reaches the Earth. This is the reason for the large uncertainty that surrounds the parameters related to the e^\pm flux produced by a PWN.

For the computation of the flux of e^\pm emitted by pulsars, we consider a source spectrum of the same form as the one in eq. (2.1). As for the SNRs, the cutoff energy E_c is expected to be in the TeV range (see refs. [165, 166]); we fix $E_c = 2$ TeV for most of our analysis of the PWN (we will comment in section 4.2 about the effect due to variation of the cut-off energy). For the spectral index, which we label γ_{PWN} , we expect a value slightly smaller than 2 (i.e. in the range [1.3 - 2]) in agreement with the mean spectral index of the gamma-ray pulsars listed in the FERMI-LAT catalog [167]. The normalization of the spectrum, Q_0 can be fixed through the total spin-down energy W_0 emitted by the pulsar [14, 168]:

$$\int_{E_{\min}}^{\infty} dE E Q(E) = \eta W_0 \quad (2.3)$$

The total spin-down energy W_0 can be expressed as:

$$W_0 \approx \tau_0 \dot{E} \left(1 + \frac{t_*}{\tau_0} \right)^2 \quad (2.4)$$

and depends on the spin-down luminosity (i.e. the energy-loss rate) \dot{E} , the present age of the pulsar t_* and the typical pulsar decay time τ_0 . The first two parameters are found in the pulsar ATNF catalog [135], while τ_0 is fixed to 10 kyr for all the sources [10, 14]. We fix $E_{\min} = 0.1$ GeV, $\gamma_{\text{PWN}} = 1.9$ and $\eta = 0.032$, if not differently stated. With these numbers, we can derive the spectral normalization Q_0 and therefore compute the e^\pm spectrum produced and accelerated inside a PWN.

2.3 Secondary positron and electrons

Secondary electrons and positrons originate from the spallation reactions of hadronic CR species (mostly protons and α particles) with the interstellar material (mostly made of hydrogen and helium). Since secondary positrons and electrons originate from positively charged ions, charge conservation implies a greater production of positrons with respect to electrons [171]. We have thoroughly discussed the production of secondary electrons and positrons in ref. [12, 14], to which we refer for any detail. Here we only recall that the steady state source term for secondaries has the form:

$$q_{e^\pm}(\mathbf{x}, E_e) = 4\pi n_{\text{ISM}}(\mathbf{x}) \int dE_{\text{CR}} \Phi_{\text{CR}}(\mathbf{x}, E_{\text{CR}}) \frac{d\sigma}{dE_e}(E_{\text{CR}}, E_e), \quad (2.5)$$

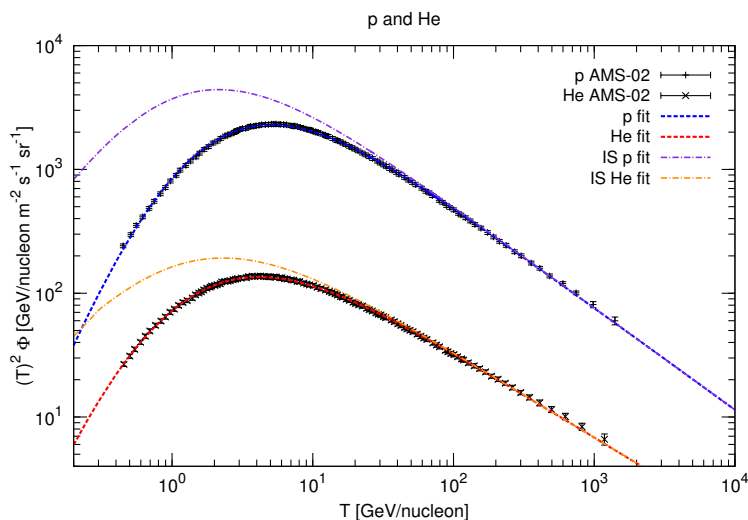


Figure 1. Primary interstellar (dot-dashed) and solar modulated (dashed) fluxes of protons (upper flux) and helium (lower flux) in function of the kinematic energy per nucleon T . Data points refer to the recent AMS-02 measurements [169, 170], dashed lines show out best fit to the data sets.

where n_{ISM} is the interstellar gas density, the primary incoming CR fluxes are denoted by Φ_{CR} , and $d\sigma/dE_e$ refers to the leptonic part of the inclusive nucleon-nucleon cross section. With respect to ref. [14], we have computed eq. (2.5) by fixing here the proton and helium primary fluxes to the new measurements of AMS-02 [169, 170]. We fit the solar-modulated data by assuming interstellar proton and He fluxes described by the function $\Phi = A\beta^{P_1}R^{-P_2}$, where $R = pc/Z$ is the rigidity of the nucleus of charge number Z and momentum p , and solar modulation described by the force-field method. We obtain: $A = 22450 \pm 560 \text{ m}^{-2}\text{s}^{-1}\text{sr}^{-1}(\text{GeV}/n)^{-1}$, $P_1 = 2.32 \pm 0.56$ and $P_2 = 2.8232 \pm 0.0053$ for the proton flux, and $A = 5220 \pm 110 \text{ m}^{-2}\text{s}^{-1}\text{sr}^{-1}(\text{GeV}/n)^{-1}$, $P_1 = 1.34 \pm 0.27$ and $P_2 = 2.6905 \pm 0.0043$ for the helium flux (and for a Fisk solar modulation potential of $615 \pm 30 \text{ MV}$). The results of our fits on the primary proton and helium fluxes, compared to the AMS data, are shown in figure 1. The best-fit chi-squared value, for 236 data points and 7 degrees of freedom, is $\chi^2/\text{d.o.f.} = 0.17$. Let us mention that a determination of the interstellar proton spectrum free from solar modulation effects could be derived by using diffuse γ -ray data: this technique has been discussed and undertaken, in a preliminary analysis, in refs. [172, 173], where a break in the interstellar spectrum around a few GeV is found.

We consider the p-p cross section parameterization described in ref. [171], which includes additional processes (especially resonances other than the Δ at low interaction energies) and has been calibrated with recent data. For reactions including helium, both as a target and as the incoming particle, we use the empirical prescription and the results described in ref. [12].

3 The propagation of electrons and positrons in the Galaxy

Once produced in their respective sources, electrons and positrons propagate throughout the Galaxy, where they diffuse on the magnetic field inhomogeneities. Most importantly, they lose their energy by electromagnetic interactions with the interstellar radiation field (ISRF) through inverse Compton (IC) scattering, and by synchrotron emission on the galactic mag-

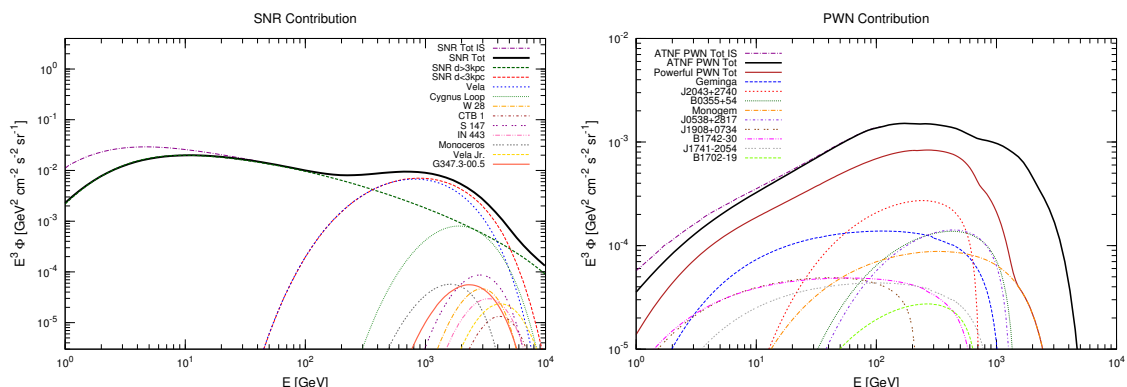


Figure 2. *Left:* Top of atmosphere electron flux (times E^3) from the nine most powerful and close (≤ 3 kpc) SNRs (from table 1), shown together with their sum (red dashed line). The green dashed line represents the electron flux from the far (> 3 kpc) SNR population, while the solid black line is the sum of all the contributions. *Right:* positron flux (the same occurs for electrons) from the nine most powerful pulsars of the ATNF catalog, along with their sum (solid red line) and the sum of the fluxes of all the pulsars of the catalogue (solid black line). Galactic propagation with the *MED* model; solar modulation parameter $\phi = 830$ MV. In both panels, the dot-dashed (violet) line refers to the interstellar flux.

netic field (notably, bremsstrahlung, ionization and Coulomb interactions on the interstellar medium are negligible and can be safely neglected). The diffusion equation for the electron (positron) number density $\mathcal{N} = \mathcal{N}(E, \vec{x}, t) \equiv dn/dE$ may be written as (see ref. [14] and references therein):

$$\partial_t \mathcal{N} - \vec{\nabla} \cdot \left\{ K(E) \vec{\nabla} \mathcal{N} \right\} + \partial_E \left\{ \frac{dE}{dt} \mathcal{N} \right\} = \mathcal{Q}(E, \vec{x}, t). \quad (3.1)$$

where we have neglected the effect of convection and reacceleration [12]. In this equation, $K(E)$ is the energy-dependent diffusion coefficient while dE/dt is the energy-loss term and $\mathcal{Q}(E, \vec{x}, t)$ denotes the source term (discussed in the previous section). The solution to eq. (3.1) is found within a semi-analytical model in which the Galaxy is shaped as a cylinder, made of the stellar thin disk (with half-height of 100 pc), and a thick magnetic halo whose height L varies from 1 to 15 kpc [174]. In our analysis we closely follow ref. [14], to which we refer for any detail. We only remind here that we have included a full relativistic treatment of the IC energy losses, while for the synchrotron emission we have set the magnetic field to $1 \mu\text{G}$. The spatial diffusion coefficient $K(E) = \beta K_0 (\mathcal{R}/1 \text{ GV})^\delta$ is set to one of the three benchmark sets of parameters derived in ref. [175] and compatible with the boron-to-carbon analysis [174]. Namely, for the *MIN/MED/MAX* models we fix $\delta = 0.85/0.70/0.46$, $K_0 = 0.0016/0.0112/0.0765 \text{ kpc}^2/\text{Myr}$ and $L = 1/4/15 \text{ kpc}$, respectively. Finally, for the solar modulation affecting low energy (about $< 10 \text{ GeV}$) charged CRs, we use the force field approximation [176, 177], with a solar modulation parameter ϕ determined within our fitting procedure on the electron and positron data sets. Apart from the force field approximation, more complex models, in which solar modulation is assumed to depend on the sign of the particles charge, have been employed (see, for example, refs. [178, 179]).

We show in figure 2 the electron and positron fluxes produced from SNR and pulsars, propagated according to the above prescriptions, for the *MED* propagation parameters. The left panel shows the electron flux from the nine most-powerful among the near (≤ 3 kpc

around the Solar System) SNRs, along with the sum of their single fluxes. The source parameters have been derived from table 1, as explained in section 2.1. We also plot the contribution from the average population of distant (> 3 kpc) SNR, whose spectral index γ and normalization Q_0 have been fixed to 2.38 and $2.75 \times 10^{50} \text{ GeV}^{-1}$, respectively, according to the results of the fit on the AMS-02 data explained in the next section 4. As expected, the far SNRs contribute predominantly to the electron flux up to about 100 GeV, above which the local sources dominate. We observe that Vela(XYZ) — a near, young and strong radio-emitter SNR — is the dominant contributor, exhibiting an electron flux much higher than the other SNRs. In the right panel, we plot the positron flux (which is the same as for electrons) from the nine most powerful pulsars of the ATNF catalog, their sum and the sum of the fluxes of all the pulsars of the catalogue. We display also the top of atmosphere (solid black line) and interstellar (dot-dashed violet line) total contribution for both SNR and PWN emission. Again, the source parameters are fixed according to the analysis performed in section 4: $\gamma_{\text{PWN}} = 1.90$ and $\eta = 0.032$. The two highest fluxes in the AMS-02 high-energy range are provided by Geminga and J2043-2740, but do not really dominate over the other ones. We also observe that the flux of the most powerful PWN is indeed lower (by a factor of two up to an order of magnitude) than the flux provided by the whole PWN in the ATNF catalog. As a consistency check, we point out that our positrons and electrons interstellar fluxes appear to be in good agreement with the determination of these fluxes given in refs. [180] and [181] as the result of an analysis based on synchrotron observations, thus completely independent from any detail concerning solar modulation.

4 Fit to AMS-02 data: method and free parameters

The AMS-02 Collaboration has recently published data about the positron fraction ($e^+/(e^+ + e^-)$) [6] and presented preliminary results on the electron, positron and electron plus positron flux [7, 8]. For the latter three quantities, for which a specific information on the experimental uncertainty is not currently available, we assume an energy independent error of 8%, comprehensive of statistical and systematic uncertainties. We employ all the four observables ($e^+ + e^-$, e^- , e^+ , $e^+/(e^+ + e^-)$) in order to explore whether a unique source-model can explain AMS-02 data.

Our model is built up by the components described in section 2: *i*) electrons produced by near SNRs treated as individual sources; *ii*) electrons from an average population of distant SNR; *iii*) electrons and positrons from PWN, considered as individual sources; *iv*) secondary electrons and positrons produced by the spallation of p and He primary cosmic rays. For the electrons produced by the closest (≤ 3 kpc) SNRs, we derive their source parameters according to the prescriptions given in section 2.1 and employ the radio, distance and age data listed in table 1. For the electrons arriving to the Earth from the population of far (> 3 kpc) SNRs, we proceed as described in section 2.1, leaving the spectral index γ and the overall normalization Q_0 as free parameters. The ATNF catalog pulsars are included here by making the simplifying hypothesis that they all shine with a common spectral index γ_{PWN} and efficiency η , following the discussion outlined in section 2.2. Finally, the secondary positrons and electrons are computed from the observed primary p and He (see section 2.3), and do not depend on any free parameter. However, we allow the normalization to be adjusted (by an overall renormalization factor that we call here \tilde{q}_{sec}) in the fit to the AMS-02 data, in order to verify *a-posteriori* if the secondary positron production (determined by CR hadrons) is consistent with the measured lepton data. In summary, the free parameters of the model

are: γ , Q_0 , γ_{PWN} , η , \tilde{q}_{sec} and ϕ , where the latter (the solar modulation potential) is let free in order to accommodate low energy data. We jointly fit all the four datasets together.

In figure 3, we show the result of the fit on all the four leptonic observables: the flux of electrons plus positrons, electrons, positrons and the positron fraction. The four panels report the total flux for each observable, together with the single subcomponents arising from the different categories of sources. Figure 3 also shows AMS-02 data and data from previous experiments. The best fit to each observable is shown as a solid line, embedded in its 3σ uncertainty band. The result of the analysis shows a quite remarkable agreement with AMS-02 data: this is confirmed by the value of the best-fit chi-squared: $\chi^2/\text{d.o.f.} = 0.65$, for 236 data points and 6 degrees of freedom. The best fit-values of the 6 parameters are: $\eta = 0.0320 \pm 0.0016$, $\gamma_{\text{PWN}} = 1.90 \pm 0.03$ for the PWN sources, $Q_0 = (2.748 \pm 0.027) \times 10^{50} \text{ GeV}^{-1}$ and $\gamma = 2.382 \pm 0.004$ for the far SNRs, the renormalization of e^+ and e^- secondary contribution is $\tilde{q}_{\text{sec}} = 1.080 \pm 0.026$, and the Fisk potential turns out be 830 ± 22 MV. The value of Q_0 is similar to the one derived in section 2.1 for the 88 sources of the Green catalog with measured radio index, flux and distance.

The various electrons and positrons sources have different impact in the reconstruction of the properties of the four set of observables. At high energies, local sources are the most relevant: SNR for the electron flux and the $(e^+ + e^-)$ total flux, PWN for the positron flux and, in turn, the positron fraction; at lower energies, far SNR are dominating the flux of electrons and of $(e^+ + e^-)$ (this occurs for energies below about 100 GeV), while secondaries determine the positron flux and the positron fraction (for energies below 10-20 GeV). It is therefore remarkable that a single model for all the source components, for both positron and electrons, fits simultaneously all the leptonic AMS-02 data, without any further ad-hoc adjustment. The best fit values found for the free parameters of SRN and PWN are in very good agreement with the ones quoted in sections 2.1 and 2.2.

Another quite interesting result concerns the positron flux interpretation. The secondary positron component adopted in our analysis, as discussed above, depends only on the p and He primary fluxes (which we have determined by a separate, independent, fit on the recent AMS-02 data), on the nuclear cross sections involved in the spallation process and on propagation in the Galaxy. Therefore, this component does not require additional assumptions (like it is in the case of the SNR and PWN contributions, which have free unknown parameters), and is therefore somehow fixed once a specific propagation model is assumed. In order to check *a posteriori* the compatibility with the AMS-02 data, we have allowed the normalization parameter \tilde{q}_{sec} to freely vary: the fact that we find a best-fit value of \tilde{q}_{sec} very close to one, for the *MED* propagation parameters, is a confirmation of the good level of consistency in the analysis. A further discussion of the secondary positron component is given in the next section.

4.1 The case for secondary positrons

The positron spectra is interpreted in terms of a secondary production at low energy and of a PWNs emission at higher (>10 GeV) energies. As already recalled, the secondary positrons depend on their progenitor p and He spectra, on the involved spallation cross sections, and on the propagation in the Galaxy. The uncertainties of the first two ingredients are definitely smaller than the ones induced by propagation. We study here the effect of the different *MIN*, *MED* and *MAX* models described in section 3 on the secondary and PWN positrons. This theoretical emission is then compared with the e^+ spectrum measured by AMS-02 [7].

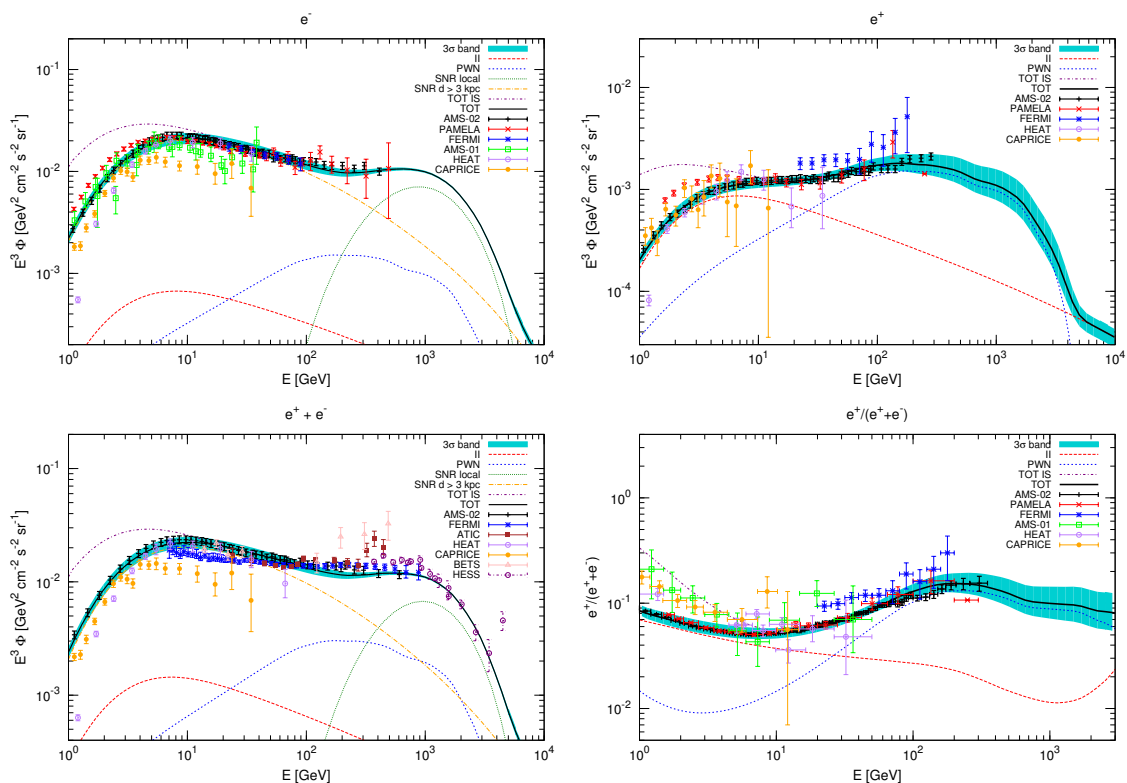


Figure 3. Results of our simultaneous fit on the AMS-02 data for the electron flux (top left), positron flux (top right), electron plus positron flux (bottom left) and positron fraction (bottom right). The best fit model is represented by the solid black line, and is embedded in its 3σ uncertainty band (cyan strip). In each panel, the dot-dashed yellow line represents the electron flux from the far (>3 kpc) SNR population, the dotted green line the electrons from the local SNRs, while the short dashed blue line describes the positron and electron flux from PWN and the long dashed red takes into account the secondary contribution to both electron and positron flux. The fit is performed on all the AMS-02 data simultaneously. Together with our theoretical model, data from AMS-02 [6–8], Fermi-LAT [4, 5], Pamela [1–3], Heat [182–185], Caprice [186, 187], Bets [188, 189] and Hess experiments [46, 190] are reported. Long-dashed lines report the corresponding interstellar fluxes, before solar modulation.

We derive the secondary and PWNs production of positrons considering the *MIN*, *MED*, *MAX* propagation models and fit the measured spectrum of positrons with the Fisk potential ϕ , the efficiency η and the index γ_{PWN} for PWN as free parameters. We have allowed the Fisk potential to vary in the range (0.6, 1.0) GV, in accordance to results¹ of combined analysis of proton and helium spectra correlated with neutron monitors data [191, 192], and compatible with our determination for the AMS-02 data taking period derived in section 2.3 with the fit on AMS-02 proton and helium fluxes.

The positron spectra are displayed in figure 4 for *MIN*, *MED* and *MAX* models, and for the secondary, PWNs and total spectra. The best fit values for the Fisk potential are 0.6, 0.77 and 1.0 GV, for the PWNs efficiency 0.011, 0.032 and 0.087 while for γ_{PWN} are 1.43, 1.90 and 2.08 for the *MIN*, *MED*, *MAX* respectively. Notice that in the case of *MIN* and *MAX* the Fisk potential best fit values are the minimal and maximal allowed in this analysis. The best-fit chi-squared is for 56 data points and 3 degrees of freedom $\chi^2/\text{d.o.f.} = \{2.43, 0.66, 4.62\}$ for

¹http://cosmicrays.oulu.fi/phi/Phi_mon.txt.

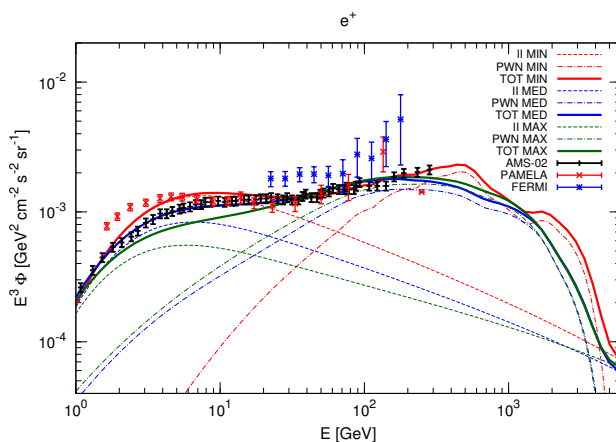


Figure 4. The positron spectrum for the *MIN* (red), *MED* (blue) and *MAX* (green) propagation models are displayed together with AMS-02, Fermi-LAT [4, 5] and Pamela [2] data. The theoretical contribution has been derived for the secondary (dashed), PWNs (dot-dashed) and total spectra (solid).

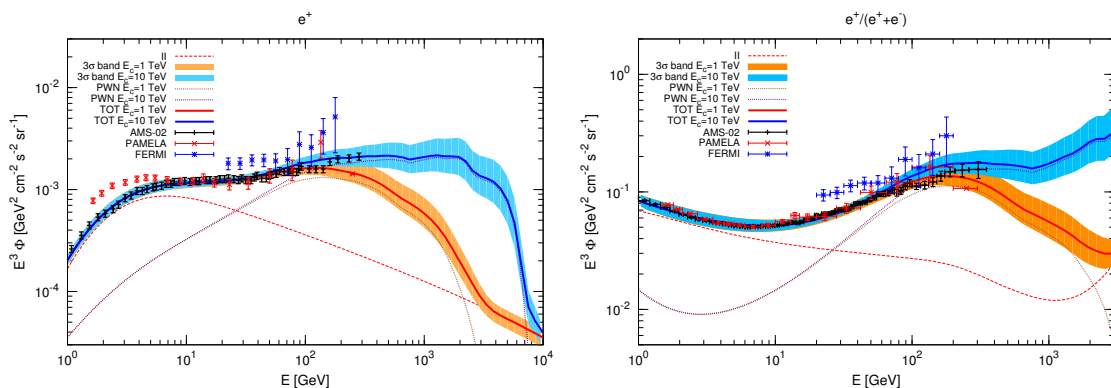


Figure 5. Positron flux (left) and positron fraction (right) for two different extreme values of the cut-off energy of pulsars: $E_c = 1$ TeV (lower red curve) and $E_c = 10$ TeV (upper blue curve). The curves show the best-fit agreement with the whole AMS-02 data set; the band around each curve represents the 3σ allowed range. AMS-02 [6, 7], Fermi-LAT [4, 5] and Pamela [1, 2] data are displayed together with theoretical expectations.

the *MIN*, *MED*, *MAX*. We see that the *MED* set of parameters predicts a positron spectrum fully compatible with the data, as previously derived in section 4. On the other hand, the *MIN* (*MAX*) are not compatible with the data, mostly because of the low energy secondary positrons, which depend sensibly on galactic diffusion. We have checked that one would need to renormalize the secondary component by a factor $\tilde{q}_{\text{sec}} = 0.72$ (1.78) for the *MIN* (*MAX*) cases, in order to reproduce the e^+ AMS-02 measurements below 10 GeV. Remarkably, the *MIN* model predicts an exceedingly high positron flux and indicates that a small halo size together with a very soft diffusion coefficient are strongly disfavored by low energy positron data.

4.2 The case for pulsars cut-off energy

The high-energy part of the positron data (positron flux and positron fraction) is of special interest, since it might disclose relevant information on their source (including a very intriguing dark matter origin). We have examined the impact of the uncertain cut-off energy in pulsar emission. Figure 5 shows the positron flux and the positron fractions calculated under two extreme situations (which encompass the case adopted in all other analysis in this paper, i.e. $E_c = 2$ TeV): the lower red curve shows the best-fit to the whole AMS-02 data when we assume $E_c = 1$ TeV; the upper blue curve is the best-fit obtained when $E_c = 10$ TeV. The band around each curve represents the 3σ allowed range. We notice that current data, which extend up to about 300 GeV, can be explained remarkably well for a wide interval of variation for E_c : they are not yet sensitive to the drop expected from the exponential cut-off, and the expectation for the positron flux and for the positron fraction above the current AMS-02 highest energy, suggest a either a mild decrease (for E_c close to 1 TeV) or even an almost constant value up to energies well above the TeV scale (for E_c close to 10 TeV). An increase in positron fraction is not likely to be expected in the 300 – 1000 TeV energy range. Notice that the positron fraction at these energies depends also on the cut-off energy of SNR, discussed in section 2.1: however, the electron+positron flux measured up to energies of few TeV by HESS, points toward a value around 2 TeV (as can be seen in figure 3) and therefore it does not appear to be allowed to substantially vary, and therefore alter the positron fraction shown in figure 5. We also wish to comment that the two extreme values adopted here for the pulsars cut-off energy are representative cases, adopted to encompass the possible maximal effect. Expected values for E_c should be more close to a few TeV, at most.

From figure 5 we can also observe that a sharp drop in the positron observables just above the current AMS-02 highest energy could hardly be attributed to a pulsar origin: it would therefore represent an interesting clue to a positron exotic origin, like dark matter annihilation or decay in a hard production channel. On the contrary, if pulsars are a major contributor at the current experimental energies, it would be difficult to have a clear signal of dark matter at higher energies, unless dark matter is very heavy.

5 High-energy window and local sources

In this section we attempt additional analyses of the full set of AMS-02 observables, with a special attention to the interpretation of the higher energy window. Data above about 10 GeV are of special interest, since they clearly show a rise in the positron fraction, which is due to a positron production at high energies much larger than what is expected by secondary interactions only. The analysis of section 4 shows that this can be ascribed to the positron emission from local pulsars. In section 4 we considered the whole integrated contribution from the PWN reported in the ATNF catalog, where each pulsar was tuned to its catalog parameters as far as the spin-down energy W_0 is concerned, while the spectral index γ_{PWN} and the efficiency η of e^\pm emission were allowed to vary, but they were assumed to be common to all the PWN in the catalog (the actual values of these two parameters were then determined by the fit).

In this section we attempt a more detailed inspection of the PWN contribution, and to this aim we carry out two different analyses, with somewhat opposite strategies. In the first approach (called “single-source” analysis) we try to understand if a single, powerful, pulsar among the ones present in the ATNF catalog, is able alone to properly explain the high-energy part of the AMS-02 data, still retaining, in the global analysis, a good agreement

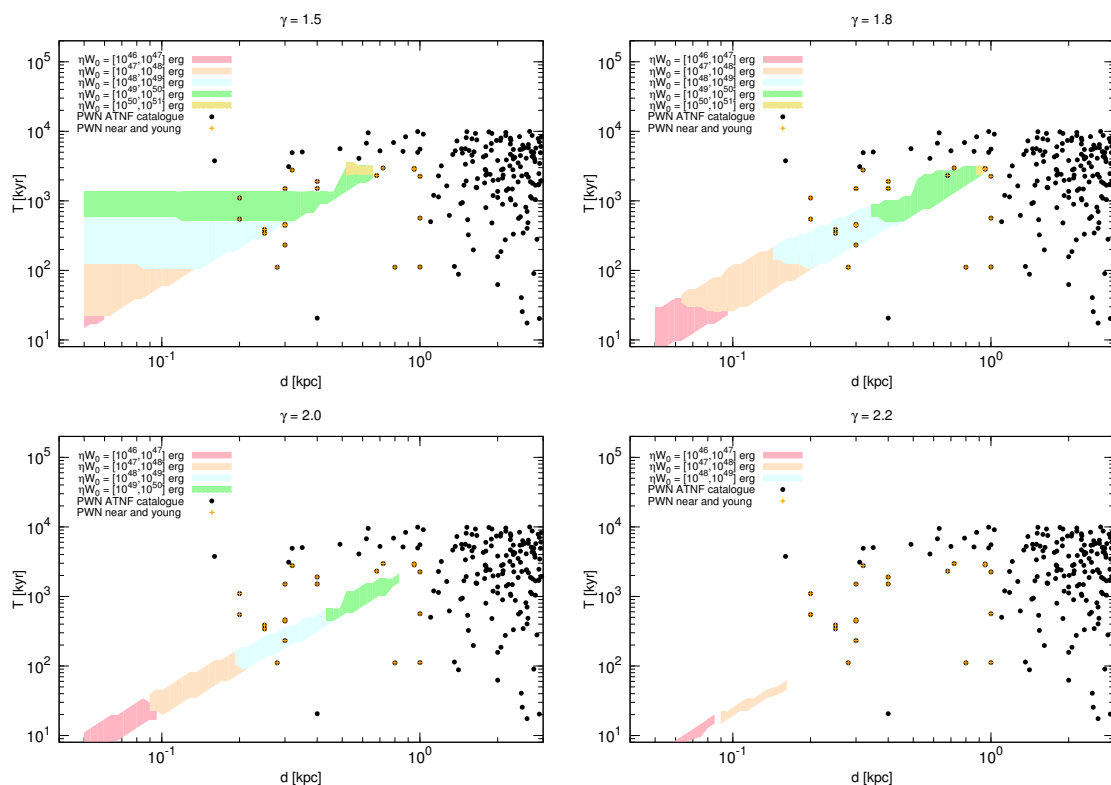


Figure 6. “Single-source” analysis. The colored areas correspond to the 3σ allowed regions, in the single-PWN parameter space, compatible with the four observables measured by AMS-02. The different panels refer to four representative values of the spectral index: $\gamma_{\text{PWN}} = 1.5, 1.8, 2.0, 2.2$. Bands of different colors correspond to various decades of values for the parameter ηW_0 , as reported in the insets (from the lower to the upper band: $(10^{46}, 10^{47})$ erg, $(10^{47}, 10^{48})$ erg, $(10^{48}, 10^{49})$ erg, $(10^{49}, 10^{50})$ erg, $(10^{50}, 10^{51})$ erg, $(10^{51}, 10^{52})$ erg). The circles correspond to PWN listed in the ATNF catalogue (an orange mark differentiates PWN which are young and close, defined as PWN with $T < 3000$ kyr and $d < 1$ kpc).

in the whole energy range: in fact, we include in our analysis all the electron and positron sources and analyze the whole energy range for all the four AMS-02 observables, one of which is the single-source PWN. It is a global-fit to the AMS-02 data, where the PWN contribution is ascribed to a single source. We therefore model a generic single PWN contribution with free parameters in terms of distance d , age T , spectral index γ_{PWN} and energy released in e^\pm (i.e., the quantity ηW_0). We determine the allowed regions in the 4-dimensional parameter space (d , T , γ_{PWN} and ηW_0) and then we check in the ATNF catalogue if there are sources which are compatible with the requirements derived from this analysis. We will show that the ATNF catalogue contains a few, close and relatively (but not extremely) young PWN which can potentially have the correct properties to explain the high-energy part of the AMS-02 (and PAMELA, as well) data.

In the second analysis (called “powerful-sources” analysis) we take a different approach. We identify in the ATNF catalogue the 5 most powerful sources in terms of spin-down energy. For each of them, we adopt the distance d and age T provided in the catalogue, as well as the spin-down energy W_0 . We, instead, allow to be free parameters the efficiency η and spectral index γ_{PWN} for each one of the five PWN (in total, we therefore have 10 free parameters). By a

scan in the 10-dimensional parameter space, we derive statistical distributions of the allowed ranges of the efficiencies and spectral indexes of the five PWN. This allows to determine the preferred properties of the five pulsars and to discern if some of them are constrained to possess specific features or, at the opposite, if the data are somehow blind to PWN properties (all this, we recall, under the hypothesis that the 5 most powerful PWN are the dominant contributors). We will find that in this context, Geminga is required to have a relatively soft emission spectrum and a relatively large efficiency, regardless of the properties of the other four pulsars, which instead are allowed to span a broad band of values both for the efficiency and for the spectral index.

Finally, we extend the “powerful-sources” analysis to comprise an additional component, represented by all the other PWN listed in ATNF catalogue (a sort of additional “PWN background”): while we assume for all of them the position, age and spin-down energy reported in the catalog, we attribute to them a common spectral index and efficiency. We therefore repeat the analysis with a 12-dimensional parameter space and derive the statistical distribution of the values which allow a good fit to the AMS-02 data. In this case, we will obtain that the prominent role of Geminga is reduced (its efficiency can now be smaller than in the previous case) but the additional “background” pulsars are constrained to possess relatively small efficiencies.

Let us move now to the discussion of the two types of analyses.

5.1 “Single-source” analysis

In the “single-source” analysis we attempt to reproduce the full set of AMS-02 data by invoking a single PWN contributing to the high-energy part of the positron flux. While the SNR contribution and the secondaries are fixed at their best-fit configuration determined in section 4, pulsar emission is attributed to a single source, for which we vary the spectral index γ_{PWN} in the interval $[1.4, 2.2]$, the distance d in $[0.01, 3]$ kpc, the age T in $[1, 20000]$ kyr, and the power emitted in the electron/positron channel ηW_0 in $[10^{46}, 10^{51}]$ erg (η representing the efficiency of emission in this channel). We therefore determine the regions in this 4-dimensional parameter space which are able to reproduce the AMS-02 observables. The four panels of figure 6 show the 3σ allowed regions in the plane distance-age, at different values of the spectral index ($\gamma_{\text{PWN}} = 1.5, 1.8, 2.0, 2.2$) and for various decades of values for the parameter ηW_0 , depicted by bands of different colors (from the lower to the upper band: $(10^{46}, 10^{47})$ erg, $(10^{47}, 10^{48})$ erg, $(10^{48}, 10^{49})$ erg, $(10^{50}, 10^{51})$ erg, $(10^{51}, 10^{52})$ erg). In our 4-dimensional parameter space, the best-fit configurations has a reduced- χ^2 of 0.45 for 236 data points and 6 degrees of freedom, and the regions denote the 3σ allowed area. The figure shows that, regardless of the spectral index, only local (closer than about 1 kpc) and young (age below about 3000 kyr) sources are compatible with the AMS-02 data, and that very soft spectra would require extremely young and close PWN.

We can now verify if in the ATNF catalog we can identify sources which have the right properties to explain the AMS-02 leptonic data. This is obtained by reporting, in the same panels of figure 4, the position and age of all observed PWN with $d \leq 3$ kpc and $T \leq 10000$ kyr (an orange mark differentiates PWN which are young and close, defined as objects with $T < 3000$ kyr and $d < 1$ kpc). We can see that, depending on the spectral index and on the emission power, we can identify 9 PWN which are potentially able to explain the AMS-02 data with a high level of confidence. These PWN are listed in table 2, together with their catalog name and parameters. Table 2 also shows, for different allowed spectral indexes, the allowed interval for the effective emission power (in the electron/positron channel) $\eta W_{0,\text{fit}}$

determined by our fit (in units of 10^{49} erg). From the information on the total emitted power $W_{0,\text{cat}}$, we can infer information on the efficiency η_{fit} required by these sources in order to reproduce the data:

$$\eta_{\text{fit}} = \frac{\eta W_{0,\text{fit}}}{W_{0,\text{cat}}} \quad (5.1)$$

The last columns of table 2 reports the allowed intervals obtained for η_{fit} : we notice that in most of the cases the required emitted power is too large (i.e. η_{fit} is too large, even much larger than 1) as compared to observations. However, and most notably, in a few cases the required values of the efficiency are quite reasonable: this occurs for Geminga, for which efficiencies of the order of 0.3 – 0.4 are obtained for a wide interval of spectral indexes (ranging from 1.5 to 1.9); for B1742-30, where efficiencies of the order of 0.6 are possible in the case of hard spectra ($\gamma_{\text{PWN}} \sim 1.6 - 1.7$); and for J1741-2054, with $\eta_{\text{fit}} \sim 0.6$ for $\gamma_{\text{PWN}} \sim 1.7 - 1.8$. All other PWN instead appear quite disfavored. Although in table 2 we emphasize (in boldface) all solutions with $\gamma_{\text{PWN}} < 2$, to account for possible uncertainties in the determination of the emitted power $W_{0,\text{cat}}$, we nevertheless conclude that a “single-source” solution to the AMS-02 data is indeed possible, but only for a very limited number of PWN, namely Geminga [10, 193, 194], B1742-30 or J1741-2054.

For those three emitters, plus J1918+1541 which is the only remaining candidate which admits solution with $\gamma_{\text{PWN}} < 2$, we show in table 3 their best-fit solutions: it is remarkable (although expected from the above analysis) that the best-fit values for the distance and age of the sources reported in table 3 are quite close to the corresponding values in the ATNF catalog. From table 3 we can conclude that in the case of a single-source contributor, Geminga appears to be best option, with a derived spectral index $\gamma_{\text{PWN}} = 1.74$ and efficiency $\eta = 0.27$. The electron, positron, electron+positron fluxes and the positron flux obtained with the Geminga solution are shown in figure 7.

We wish to emphasize that, with the results of this analysis, we are not claiming that we have unambiguously identified the source of the high-energy positron flux (equivalently good solutions have been obtained in section 4, where all pulsars in the ATNF catalog are contributing, and others will be found in the next section with the “powerful sources” analysis). Instead, we attempted to investigate if a solution in terms of a single emitter is possible and if the ATNF catalog contains viable candidates, which indeed occurs. A verification that the sources reported in table 3 have the spectral index and efficiency quoted in the table would require additional observational data. At the same time, we wish to comment that the use of catalog sources might be biased from incompleteness of the catalog. The ATNF catalog might not (and very likely, does not) contain all local PWN, since for a fraction of them the electromagnetic emission may not be resolved. This might occur for the SNR in the Green catalog, as well. Nevertheless, it is remarkable that current data can be properly and fully explained in terms of known sources. In the case of the “single-source analysis” discussed in this section, the results of figure 6 can also be interpreted as bringing information on the age-distance parameters required for any unknown single, powerful PWN to explain the AMS-02 leptonic data: any putative source likely needs to be closer than 1 kpc and younger than about 3000 kyr, with specific correlations with its spectral index and emitted power, as reported in the panels of figure 6.

5.2 “Powerful-sources” analysis

In this section we adopt a somehow complementary approach to the “single-source analysis” discussed in section 5.1: we identify, in the ATNF catalog, a limited number of PWN which

Name	d_{cat}	T_{cat}	$W_{0,\text{cat}}$	γ_{PWN}	$\eta W_{0,\text{fit}}$	η_{fit}
B1742-30	0.20	546	0.829	1.4	(0.85,1.2)	<i>(1.0,1.5)</i>
				1.5	(0.61,1.00)	<i>(0.79,1.2)</i>
				1.6	(0.52,0.85)	<i>(0.63,1.0)</i>
				1.7	(0.52,0.61)	<i>(0.63,0.74)</i>
B1749-28	0.20	1100	0.700	1.4	(2.3,3.2)	(3.3,4.6)
				1.5	(1.9,2.7)	(2.71,3.86)
				1.6	(1.4,1.9)	(2.0,2.7)
Geminga	0.25	342	1.25	1.5	(0.44,0.61)	<i>(0.35,0.41)</i>
				1.6	(0.32,0.52)	<i>(0.26,0.42)</i>
				1.7	(0.27,0.44)	<i>(0.22,0.35)</i>
				1.8	(0.27,0.37)	<i>(0.22,4.57)</i>
				1.9	(0.32,0.37)	<i>(0.26,0.30)</i>
J1741-2054	0.25	386	0.470	1.5	(0.44,0.61)	<i>(0.94,1.1)</i>
				1.6	(0.32,0.52)	<i>(0.68,1.1)</i>
				1.7	(0.27,0.44)	<i>(0.57,0.94)</i>
				1.8	(0.27,0.52)	<i>(0.57,1.1)</i>
B0959-54	0.30	443	0.044	1.5	(0.72,0.85)	(16,19)
				1.6	(0.44,0.85)	(10,19)
				1.7	(0.44,0.72)	(10,16)
				1.8	(0.44,0.61)	(10,14)
				1.9	(0.37,0.52)	(8.4,12)
B0940-55	0.30	461	0.217	1.5	(0.72,0.85)	(3.3,3.9)
				1.6	(0.44,0.85)	(2.0,3.9)
				1.7	(0.44,0.72)	(2.2,3.3)
				1.8	(0.44,0.61)	(2.0,2.8)
				1.9	(0.44,0.52)	(2.0,2.4)
B0834+0	0.72	2970	0.364	1.6	(8.4,10)	(23,28)
				1.7	(7.2,8.5)	(20,4.23)
J1918+1541	0.68	2310	3.39	1.6	(6.1,10)	<i>(1.8,2.9)</i>
				1.7	(5.1,8.5)	<i>(1.5,2.5)</i>
				1.8	(4.4,6.1)	<i>(1.3,1.8)</i>
				1.9	(6.1,7.2)	<i>(1.8,2.2)</i>
B1822-09	0.30	232	0.0849	1.8	(0.19,0.27)	(2.2,3.2)
				1.9	(0.23,0.32)	(2.7,3.8)
				2.0	(0.23,0.32)	(2.7,3.8)
				2.1	(0.32,0.37)	(3.8,4.4)

Table 2. “Single-source” analysis. List of the pulsars reported in the ATNF catalogue whose distance and age lie inside the regions of parameter space compatible with AMS-02 measurements, identified by our single-source analysis (for a few representative values of the spectral index γ_{PWN} , these pulsars are those shown in figure 6 which fall inside the reconstructed regions). The columns report the pulsar catalog name, the distance d_{cat} (in kpc), age T_{cat} (in kyr) and total emitted power $W_{0,\text{cat}}$ (in units of 10^{49} erg) reported in the ATNF catalog, the spectral index γ_{PWN} , the range of the emissivity $\eta W_{0,\text{fit}}$ for which the source is able to reproduce the AMS-02 observables and finally the reconstructed value of the pulsar efficiency which is required to match the emissivity $W_{0,\text{cat}}$ (in italic, we emphasize those cases where this effective efficiency parameter is smaller than 2).

are potentially able to sizably contribute to the local positron flux at high-energies, and we use them in the global analysis of the full set of AMS-02. For definiteness, we adopt the 5 “most powerful” sources, and for each of them we allow a free spectral index γ_{PWN} and a free efficiency factor η , which are then determined by fitting the AMS-02 data. All the

Name	γ_{fit}	d_{fit}	T_{fit}	$\eta W_{0,\text{fit}}$	χ^2/dof	d_{cat}	T_{cat}	$W_{0,\text{cat}}$	η_{fit}
Geminga	1.74	0.24	344.6	0.341	0.68	0.25	342	1.25	0.27
J1741-2054	1.68	0.25	378.0	0.413	0.62	0.25	386	0.47	0.88
B1742-30	1.52	0.19	539.1	0.770	0.54	0.2	546	0.83	0.92
J1918+1541	1.65	0.64	2355	6.48	0.92	0.68	2310	3.4	1.90

Table 3. “Single-source” analysis. For the four PWN identified in the “single-source” analysis as those which can provide the best agreement to the AMS-02 data (the ones that in table 2 exhibit an effective efficiency smaller than 2), we report here the best-fit values obtained for their spectral index γ_{fit} , distance d_{fit} (in kpc), age T_{fit} (in kyr) and emitted power $\eta W_{0,\text{fit}}$ (in units of 10^{49} erg), and for comparison the catalog values of distance d_{cat} , age T_{cat} and power $W_{0,\text{cat}}$. From $\eta W_{0,\text{fit}}$ and $W_{0,\text{cat}}$ we derive the efficiency η_{fit} .

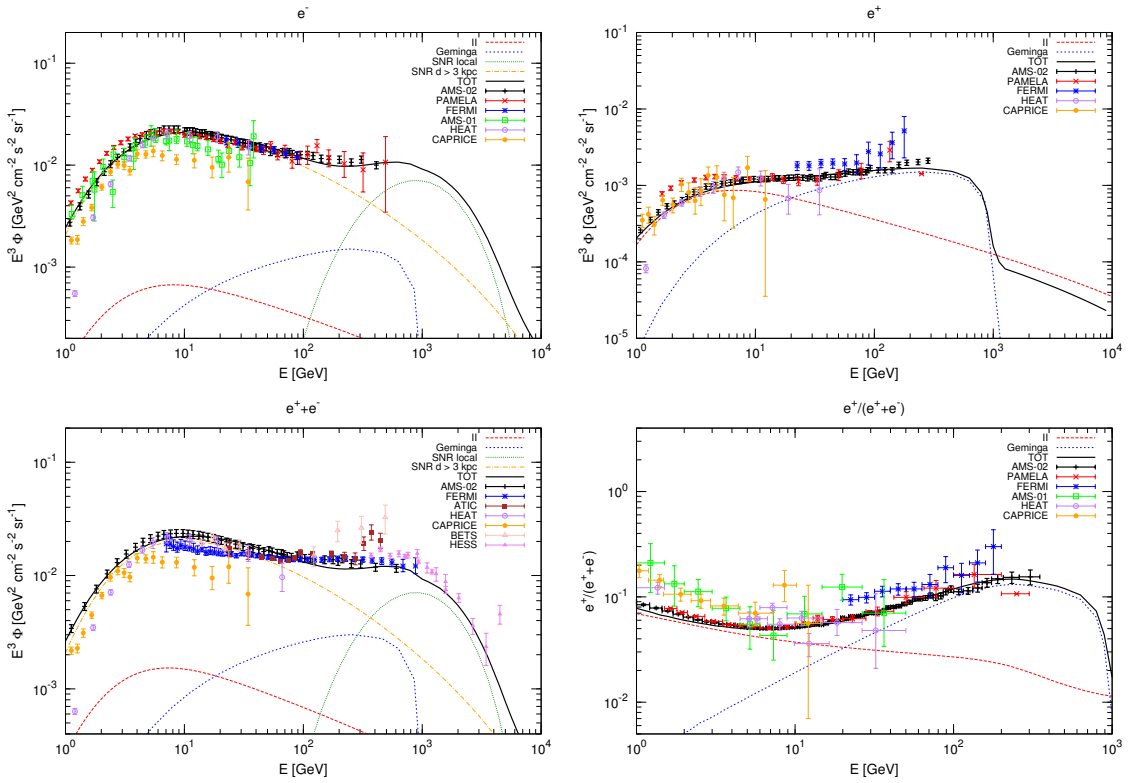


Figure 7. “Single-source” analysis. Results of our simultaneous fit on the AMS-02 data for the electron flux (top left), positron flux (top right), electron plus positron flux (bottom left) and positron fraction (bottom right) when the pulsar contribution is fully supplied by Geminga alone. The fit is performed on all the AMS-02 data simultaneously and the derived Geminga parameters are those reported in table 3. The colors and styles of the lines are the same as in figure 3. Together with our theoretical model, data from AMS-02 [6–8], Fermi-LAT [4, 5], Pamela [1–3], Heat [182–185], Caprice [186, 187], Bets [188, 189] and HESS experiments [46, 190] are reported.

other leptonic components (SNR and secondaries) are taken at their best-fit configuration of section 4, for definiteness. We label this analysis “powerful-sources” analysis.

The criterion used to identify the 5 “most powerful” sources relies on a ranking-algorithm based on the contribution of the PWN to the high-energy part of the positron flux. Since

ATNF	Association	d [kpc]	T [kyr]	W_0 [10^{49} erg]
J0633+1746	Geminga	0.25	343	1.26
J2043+2740		1.13	1204	26.0
B0355+54		1	567	4.73
B0656+14	Monogem	0.28	112	0.178
J0538+2817		1.3	622	6.18

Table 4. “Powerful-sources analysis”. List of the 5 pulsars identified as “most-powerful” with the criteria defined in the text, as used in the analysis. The columns report the ATNF-catalog name, the association name, the distance d [kpc], the age T [kyr] and the emitted power W_0 (in units of 10^{49} erg), as reported in the catalog.

pulsars contribution becomes dominant above about 10 GeV, we have subdivided the energy range (10 – 550) GeV into 4 equally spaced in log-scale bins, and for each bin we have calculated the integrated positron flux for all the PWN present in the ATNF catalog, by adopting for them a common spectral index and efficiency (taken at the best-fit values of section 4). By using the calculated fluxes Φ_i^a ($i = 1, \dots, 4$ counts the energy bins, a counts the PWN in the catalog) we have created a rank R_i^a of the sources a in each bin i ($R_i^a = 1, 2, \dots$ for the most-powerful, second most-powerful, and so on). The 5 “most-powerful” sources are then identified as those who possess the highest ranking $\bar{R}^a = \sum_i R_i^a$ (i.e. the smaller value of \bar{R}^a). These pulsars are listed in table 4.

Now that we have identified the PWN to be used in the analysis, we allow for them a variation of the spectral index γ_{PWN} and efficiency η parameters, while assuming their distance d , age T and total emitted power W_0 at their catalog values. The analysis therefore relies on 10 free parameters, which are varied independently. By fitting the whole set of AMS-02 data, we can identify the best-fit configuration and the corresponding 3σ allowed region in this 10-dimensional parameter space. For those configurations falling in the 3σ allowed region, figure 8 shows the frequency distribution of the two parameters for each of the 5 “most-powerful” sources. We can notice that there is a preferred trend for Geminga: the efficiency is required to be larger than about 0.1, with a peak value around 0.2 – 0.3 (not far from the best-fit value 0.27 obtained in the “single-source” analysis) and that its spectral index is lower-bounded arounded 1.6, with a small (but not significant) preference toward softer spectra (we can notice that in the case Geminga is the only, largely dominant, contributor the “single-source” analysis has determined a best-fit value of 1.74). The other four “most-powerful” PWN are much less constrained: they have a mild preference for efficiencies lower than 0.1 and no clear preference for the value of the spectral index.

In order to understand the role of the additional PWN present in the ATNF catalog, we have performed an extended version of the “power-source” analysis where, in addition to the 5 sources defined above, we have added the contribution of all the remaining pulsars in the catalog (a sort of “PWN background”, just to fix a denomination): for each of them, we adopt a common spectral index and efficiency, while the other 3 parameters (d , T , and W_0) are taken at the value reported in the catalog. The analysis now deals with 12 parameters. We have again performed a fit on the whole set of AMS-02 data, identified the 3σ allowed regions around the best-fit configuration on the 12-dimensional parameter space: figure 9 shows the frequency distribution of the values of γ_{PWN} and η for each of the 5 “most-powerful” pulsars, as well as the frequency distribution of the spectral index and efficiency of the pulsars

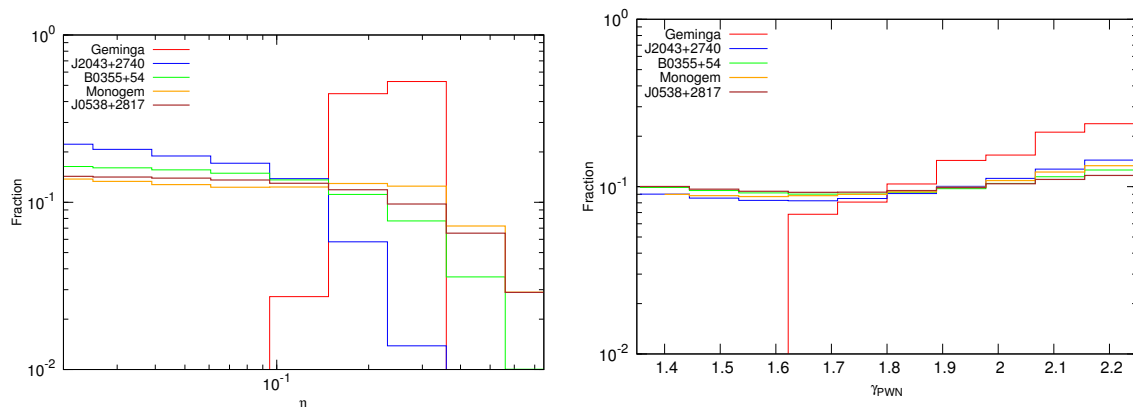


Figure 8. “Powerful-source analysis”. Frequency distribution of the values of the efficiency η (left) and the spectral index γ (right) of the five “most powerful” sources. The distributions refer to the PWN configurations which lie inside the 3σ allowed region around the best-fit configuration on the AMS-02 full data set.

contributing to the “PWN background”. The presence of the additional pulsars makes the role of Geminga less relevant, as can be seen by the fact that now the allowed interval for the efficiency is widely distributed, contrary to the previous case: while the most probable value is still around $0.1 - 0.2$, much lower efficiencies are now accepted, while only efficiencies in excess of 0.1 were accepted with a negligible contribution of the “PWN background”. The additional pulsars have a tendency toward low efficiencies, around 0.05 . The spectral features do not exhibit strong preferences, except for Geminga and for the “PWN background”, where a mild tendency toward soft spectra appears, as shown in the right panel of figure 9.

The kind of agreement which can be obtained with the “powerful-sources” approach can be appreciated in figure 10, where we show the best-fit configuration of the analysis for the 5 “most-powerful” pulsars for the combined analysis of the electron flux (top left), positron flux (top right), electron plus positron flux (bottom left) and positron fraction (bottom right). All four data sets are reproduced quite well, with a similar level of agreement already obtained with the other approaches discussed above. The best-fit configuration corresponds to a reduced- χ^2 of 0.41 for 236 data points and 12 free parameters. Also in this case, the agreement is remarkably good.

6 Conclusions

In this paper we have performed a combined analysis of the recent AMS-02 data on the electron flux, positron flux, electrons plus positrons flux and positron fraction, in a theoretical framework that self-consistently accounts for all the astrophysical components able to contribute to the leptonic fluxes in their whole energy range.

The primary electron contribution is modeled through the sum of an average flux produced by distant sources and the fluxes arising from the local supernova remnants in the Green catalog. The secondary electron and positron fluxes originate from interactions on the interstellar medium of primary cosmic rays, for which we have derived a novel determination by using AMS-02 proton and helium data. Finally, the pulsar wind nebulae contribution to the positron (and electron) fluxes at high energies relies on a modeling of the sources reported in the ATNF catalog (where information on age, distance and total emitted power

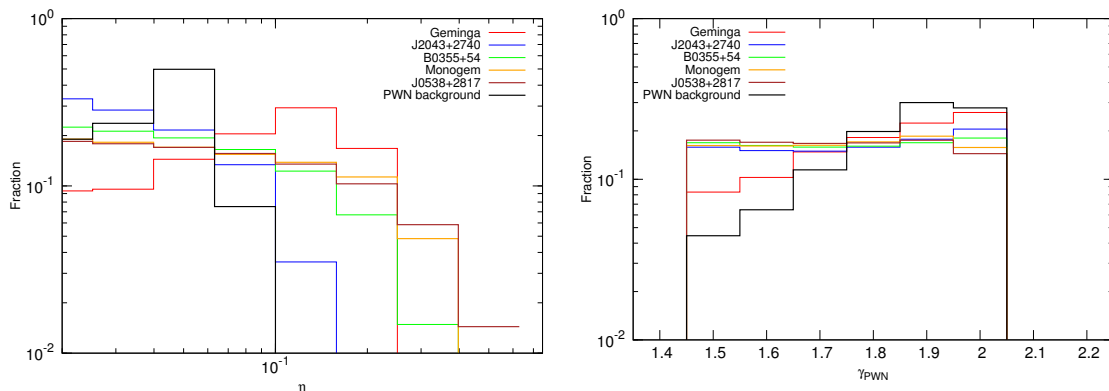


Figure 9. “Powerful-source analysis”. The same as in figure 8, with the difference that, in addition to the 5 “most-powerful” pulsars, an aggregate contribution from all the additional PWN in the ATNF catalog is added (considered as a “PWN background”). All the additional pulsars are assumed to have a common efficiency and a common spectral index.

of the pulsars is available), under a number of assumptions on the way the different pulsars might contribute to the local fluxes. We have in fact specifically performed three different type of analysis: we have studied the average contribution from the whole catalog; we have investigated if the ATNF catalog contains a single, dominant, pulsar which alone can allow agreement with the data; finally we have examined the possibility that a few powerful sources in the ATNF catalog may concurrently contribute to the local observed fluxes.

For all three different types of analysis, we obtain a remarkable agreement between our modelings and the whole set of AMS-02 data. The supernova remnants and the secondary contribution are able to properly explain the electron data and the low-energy part of the positron spectra, and to some extent they also point toward a disfavoring of small cosmic-rays confinement volumes. The high-energy part of the positron flux, which has received great attention because of its implications not only for the astrophysics of sources but also for dark matter studies, finds a remarkable solution in terms of pulsars present in the ATNF catalog. We find that AMS-02 data can be properly explained either in the case of an average contribution from the whole catalog, or for the situation where a single and close pulsar is the dominant contributor, or even in the case where a few and powerful dominant pulsars in the catalog are mostly contributing. For all cases, we have identified the required ranges of the relevant parameters (spectral index and efficiency of the emission) for the contributing pulsars, once the other parameters (age, distance, total emitted power) are fixed at their values reported in the ATNF catalog.

We can therefore conclude that the whole set of AMS-02 leptonic data admits a self-consistent interpretation in terms of astrophysical contributions. Alternative solutions, like e.g. a dark matter production of electrons and positrons, are indeed a viable alternative or complementary possibility: however, a self-consistent solution in terms of purely astrophysical sources can be properly met.

Acknowledgments

We thank Pasquale Serpico for interesting and useful discussions on the physics of supernova remnants and pulsar wind nebulae and Timur Delahaye for discussions on the study

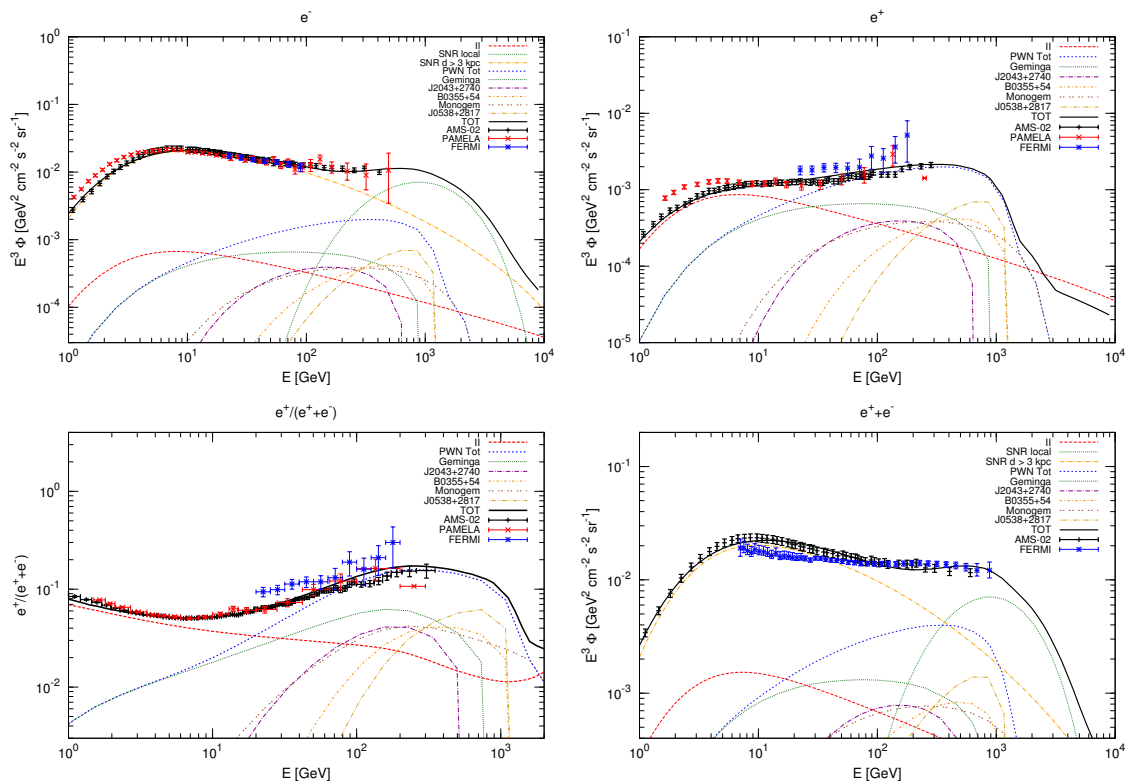


Figure 10. “Powerful-source” analysis. Results of our simultaneous fit on the AMS-02 data for the electron flux (top left), positron flux (top right), electron plus positron flux (bottom left) and positron fraction (bottom right) when the pulsar contribution is supplied by the 5 “most-powerful” pulsars in the ATNF catalog, listed in table 4. The fit is performed on all the AMS-02 data simultaneously and the result shown in the figure refers to best-fit configuration for the 5+1 efficiencies and the 5+1 spectra indexes. The colors and styles of the lines are the same as in figure 3. Together with our theoretical model, data from AMS-02 [6–8], Fermi-LAT [4, 5], Pamela [1–3], Heat [182–185], Caprice [186, 187], Bets [188, 189] and Hess experiments [46, 190] are reported.

of electron and positron cosmic rays. This work is supported by the research grant *Theoretical Astroparticle Physics* number 2012CPPYP7 under the program PRIN 2012 funded by the Ministero dell’Istruzione, Università e della Ricerca (MIUR), by the research grant *TAsP (Theoretical Astroparticle Physics)* funded by the Istituto Nazionale di Fisica Nucleare (INFN), by the *Strategic Research Grant: origin and Detection of Galactic and Extragalactic Cosmic Rays* funded by Torino University and Compagnia di San Paolo, by the Spanish MINECO under grants FPA2011-22975 and MULTIDARK CSD2009-00064 (Consolider-Ingenio 2010 Programme), by Prometeo/2009/091 (Generalitat Valenciana), and by the EU ITN UNILHC PITN-GA-2009-237920. This work is also supported in part by the European Research Council (ERC) under the EU Seventh Framework Programme (FP7/2007-2013) / ERC Starting Grant (agreement n. 278234 - ‘NEWDARK’ project). At LAPTh this activity was supported by the Labex grant ENIGMASS. R.L. is supported by a Juan de la Cierva contract (MINECO). A.V. acknowledges the hospitality of the Institut d’Astrophysique de Paris (IAP).

References

- [1] PAMELA collaboration, O. Adriani et al., *An anomalous positron abundance in cosmic rays with energies 1.5–100 GeV*, *Nature* **458** (2009) 607 [[arXiv:0810.4995](#)] [[INSPIRE](#)].
- [2] PAMELA collaboration, O. Adriani et al., *The cosmic-ray positron energy spectrum measured by PAMELA*, *Phys. Rev. Lett.* **111** (2013) 081102 [[arXiv:1308.0133](#)] [[INSPIRE](#)].
- [3] PAMELA collaboration, O. Adriani et al., *The cosmic-ray electron flux measured by the PAMELA experiment between 1 and 625 GeV*, *Phys. Rev. Lett.* **106** (2011) 201101 [[arXiv:1103.2880](#)] [[INSPIRE](#)].
- [4] FERMI LAT collaboration, M. Ackermann et al., *Measurement of separate cosmic-ray electron and positron spectra with the Fermi Large Area Telescope*, *Phys. Rev. Lett.* **108** (2012) 011103 [[arXiv:1109.0521](#)] [[INSPIRE](#)].
- [5] FERMI LAT collaboration, M. Ackermann et al., *Fermi LAT observations of cosmic-ray electrons from 7 GeV to 1 TeV*, *Phys. Rev. D* **82** (2010) 092004 [[arXiv:1008.3999](#)] [[INSPIRE](#)].
- [6] AMS collaboration, M. Aguilar et al., *First Result from the Alpha Magnetic Spectrometer on the International Space Station: Precision Measurement of the Positron Fraction in Primary Cosmic Rays of 0.5–350 GeV*, *Phys. Rev. Lett.* **110** (2013) 141102 [[INSPIRE](#)].
- [7] AMS-02 collaboration, S. Shael, *Precision measurements of the electron spectrum and the positron spectrum with AMS*, talk at 33rd ICRC Conference (2013).
- [8] AMS-02 collaboration, B. Bertucci, *Precision measurement of the electron plus positron spectrum with AMS*, talk at 33rd ICRC Conference (2013).
- [9] P.D. Serpico, *Astrophysical models for the origin of the positron ‘excess’*, *Astropart. Phys.* **39–40** (2012) 2 [[arXiv:1108.4827](#)] [[INSPIRE](#)].
- [10] D. Hooper, P. Blasi and P.D. Serpico, *Pulsars as the Sources of High Energy Cosmic Ray Positrons*, *JCAP* **01** (2009) 025 [[arXiv:0810.1527](#)] [[INSPIRE](#)].
- [11] S. Profumo, *Dissecting cosmic-ray electron-positron data with Occam’s Razor: the role of known Pulsars*, *Central Eur. J. Phys.* **10** (2011) 1 [[arXiv:0812.4457](#)] [[INSPIRE](#)].
- [12] T. Delahaye, F. Donato, N. Fornengo, J. Lavalle, R. Lineros et al., *Galactic secondary positron flux at the Earth*, *Astron. Astrophys.* **501** (2009) 821 [[arXiv:0809.5268](#)] [[INSPIRE](#)].
- [13] P. Mertsch and S. Sarkar, *Testing astrophysical models for the PAMELA positron excess with cosmic ray nuclei*, *Phys. Rev. Lett.* **103** (2009) 081104 [[arXiv:0905.3152](#)] [[INSPIRE](#)].
- [14] T. Delahaye, J. Lavalle, R. Lineros, F. Donato and N. Fornengo, *Galactic electrons and positrons at the Earth: new estimate of the primary and secondary fluxes*, *Astron. Astrophys.* **524** (2010) A51 [[arXiv:1002.1910](#)] [[INSPIRE](#)].
- [15] S. Della Torre, M. Gervasi, P. Rancoita, D. Rozza and A. Treves, *Possible Contribution to Electron and Positron Fluxes from Pulsars and their Nebulae*, [arXiv:1312.3483](#) [[INSPIRE](#)].
- [16] A. Erlykin and A.W. Wolfendale, *Cosmic ray positrons from a local, middle-aged supernova remnant*, *Astropart. Phys.* **49** (2013) 23 [[arXiv:1308.4878](#)] [[INSPIRE](#)].
- [17] D. Gaggero, D. Grasso, L. Maccione, G. Di Bernardo and C. Evoli, *PAMELA and AMS-02 positron and electron spectra are reproduced by 3-dimensional cosmic-ray modeling*, [arXiv:1311.5575](#) [[INSPIRE](#)].
- [18] D. Gaggero and L. Maccione, *Model independent interpretation of recent CR lepton data after AMS-02*, *JCAP* **12** (2013) 011 [[arXiv:1307.0271](#)] [[INSPIRE](#)].
- [19] D. Gaggero, L. Maccione, G. Di Bernardo, C. Evoli and D. Grasso, *Three-Dimensional Model of Cosmic-Ray Lepton Propagation Reproduces Data from the Alpha Magnetic Spectrometer*

- on the International Space Station, *Phys. Rev. Lett.* **111** (2013) 021102 [[arXiv:1304.6718](#)] [[INSPIRE](#)].
- [20] D. Grasso, G. Di Bernardo, C. Evoli, D. Gaggero and L. Maccione, *Galactic electron and positron properties from cosmic ray and radio observations*, [arXiv:1306.6885](#) [[INSPIRE](#)].
- [21] Q. Yuan and X.-J. Bi, *Reconcile the AMS-02 positron fraction and Fermi-LAT/HESS total e^\pm spectra by the primary electron spectrum hardening*, *Phys. Lett. B* **727** (2013) 1 [[arXiv:1304.2687](#)] [[INSPIRE](#)].
- [22] I. Cholis and D. Hooper, *Constraining the origin of the rising cosmic ray positron fraction with the boron-to-carbon ratio*, *Phys. Rev. D* **89** (2014) 043013 [[arXiv:1312.2952](#)] [[INSPIRE](#)].
- [23] M. Ibe, S. Matsumoto, S. Shirai and T.T. Yanagida, *AMS-02 Positrons from Decaying Wino in the Pure Gravity Mediation Model*, *JHEP* **07** (2013) 063 [[arXiv:1305.0084](#)] [[INSPIRE](#)].
- [24] P.S.B. Dev, D.K. Ghosh, N. Okada and I. Saha, *Neutrino Mass and Dark Matter in light of recent AMS-02 results*, [arXiv:1307.6204](#) [[INSPIRE](#)].
- [25] V.C. Spanos, *The Price of a Dark Matter Annihilation Interpretation of AMS-02 Data*, [arXiv:1312.7841](#) [[INSPIRE](#)].
- [26] A. Ibarra, A.S. Lamperstorfer and J. Silk, *Dark matter annihilations and decays after the AMS-02 positron measurements*, [arXiv:1309.2570](#) [[INSPIRE](#)].
- [27] K.R. Dienes, J. Kumar and B. Thomas, *Dynamical Dark Matter and the Positron Excess in Light of AMS*, *Phys. Rev. D* **88** (2013) 103509 [[arXiv:1306.2959](#)] [[INSPIRE](#)].
- [28] A. Hektor, M. Raidal, A. Strumia and E. Tempel, *The cosmic-ray positron excess from a local Dark Matter over-density*, *Phys. Lett. B* **728** (2014) 58 [[arXiv:1307.2561](#)] [[INSPIRE](#)].
- [29] M. Cirelli, M. Kadastik, M. Raidal and A. Strumia, *Model-independent implications of the e^\pm , anti-proton cosmic ray spectra on properties of Dark Matter*, *Nucl. Phys. B* **813** (2009) 1 [*Addendum ibid.* **B 873** (2013) 530] [[arXiv:0809.2409](#)] [[INSPIRE](#)].
- [30] Y. Zhao and K.M. Zurek, *Indirect Detection Signatures for the Origin of Asymmetric Dark Matter*, [arXiv:1401.7664](#) [[INSPIRE](#)].
- [31] S. Baek, H. Okada and T. Toma, *Radiative Lepton Model and Dark Matter with Global $U(1)'$ Symmetry*, [arXiv:1401.6921](#) [[INSPIRE](#)].
- [32] J. Kopp, L. Michaels and J. Smirnov, *Loopy Constraints on Leptophilic Dark Matter and Internal Bremsstrahlung*, [arXiv:1401.6457](#) [[INSPIRE](#)].
- [33] A. Hryczuk, I. Cholis, R. Iengo, M. Tavakoli and P. Ullio, *Indirect Detection Analysis: Wino Dark Matter Case Study*, [arXiv:1401.6212](#) [[INSPIRE](#)].
- [34] K.-Y. Choi, B. Kyae and C.S. Shin, *Decaying WIMP dark matter for AMS-02 cosmic positron excess*, [arXiv:1307.6568](#) [[INSPIRE](#)].
- [35] A. Ibarra, D. Tran and C. Weniger, *Indirect Searches for Decaying Dark Matter*, *Int. J. Mod. Phys. A* **28** (2013) 1330040 [[arXiv:1307.6434](#)] [[INSPIRE](#)].
- [36] L. Bergstrom, T. Bringmann, I. Cholis, D. Hooper and C. Weniger, *New limits on dark matter annihilation from AMS cosmic ray positron data*, *Phys. Rev. Lett.* **111** (2013) 171101 [[arXiv:1306.3983](#)] [[INSPIRE](#)].
- [37] H.-B. Jin, Y.-L. Wu and Y.-F. Zhou, *Implications of the first AMS-02 measurement for dark matter annihilation and decay*, *JCAP* **11** (2013) 026 [[arXiv:1304.1997](#)] [[INSPIRE](#)].
- [38] A. De Simone, A. Riotto and W. Xue, *Interpretation of AMS-02 Results: Correlations among Dark Matter Signals*, *JCAP* **05** (2013) 003 [[arXiv:1304.1336](#)] [[INSPIRE](#)].

- [39] L. Feng, R.-Z. Yang, H.-N. He, T.-K. Dong, Y.-Z. Fan et al., *AMS-02 positron excess: new bounds on dark matter models and hint for primary electron spectrum hardening*, *Phys. Lett. B* **728** (2014) 250 [[arXiv:1303.0530](#)] [[INSPIRE](#)].
- [40] I. Masina and F. Sannino, *Hints of a Charge Asymmetry in the Electron and Positron Cosmic-Ray Excesses*, *Phys. Rev. D* **87** (2013) 123003 [[arXiv:1304.2800](#)] [[INSPIRE](#)].
- [41] D.C. Ellison, D.J. Patnaude, P. Slane, P. Blasi and S. Gabici, *Particle Acceleration in Supernova Remnants and the Production of Thermal and Nonthermal Radiation*, *Astrophys. J.* **661** (2007) 879 [[astro-ph/0702674](#)] [[INSPIRE](#)].
- [42] V. Tatischeff, *Radio emission and nonlinear diffusive shock acceleration of cosmic rays in the supernova SN 1993J*, *Astron. Astrophys.* **499** (2009) 191 [[arXiv:0903.2944](#)] [[INSPIRE](#)].
- [43] P. Cristofari, S. Gabici, S. Casanova, R. Terrier and E. Parizot, *Acceleration of cosmic rays and gamma-ray emission from supernova remnants in the Galaxy*, *Mon. Not. Roy. Astron. Soc.* **434** (2013) 2748 [[arXiv:1302.2150](#)] [[INSPIRE](#)].
- [44] P. Blasi, *The Origin of Galactic Cosmic Rays*, [arXiv:1311.7346](#) [[INSPIRE](#)].
- [45] E.A. Helder, J. Vink, A.M. Bykov, Y. Ohira, J.C. Raymond et al., *Observational signatures of particle acceleration in supernova remnants*, *Space Sci. Rev.* **173** (2012) 369 [[arXiv:1206.1593](#)] [[INSPIRE](#)].
- [46] H.E.S.S. collaboration, F. Aharonian et al., *The energy spectrum of cosmic-ray electrons at TeV energies*, *Phys. Rev. Lett.* **101** (2008) 261104 [[arXiv:0811.3894](#)] [[INSPIRE](#)].
- [47] HESS collaboration, F. Aharonian, *Discovery of gamma-ray emission from the shell-type supernova remnant RCW 86 with H.E.S.S.*, *AIP Conf. Proc.* **1085** (2009) 332 [[arXiv:0810.2689](#)] [[INSPIRE](#)].
- [48] VERITAS collaboration, V.A. Acciari et al., *Observations of the shell-type SNR Cassiopeia A at TeV energies with VERITAS*, *Astrophys. J.* **714** (2010) 163 [[arXiv:1002.2974](#)] [[INSPIRE](#)].
- [49] HEGRA collaboration, F. Aharonian, *Evidence for TeV gamma-ray emission from cassiopeia a*, *Astron. Astrophys.* **370** (2001) 112 [[astro-ph/0102391](#)] [[INSPIRE](#)].
- [50] HESS collaboration, F. Aharonian, *Primary particle acceleration above 100 TeV in the shell-type Supernova Remnant RX J1713.7-3946 with deep H.E.S.S. observations*, *Astron. Astrophys.* **464** (2007) 235 [[astro-ph/0611813](#)] [[INSPIRE](#)].
- [51] T. Shimizu, K. Masai and K. Katsuji, *Non-Thermal Radio and Gamma-Ray Emission from a Supernova Remnant by the Blast Wave Breaking Out of the Circumstellar Matter*, *Pub. Astron. Soc. Japan* **65** (2013) 69 [[arXiv:1303.6049](#)] [[INSPIRE](#)].
- [52] I. Sushch and B. Hnatyk, *Modeling of the Radio Emission from the Vela Supernova Remnant*, *Astron. Astrophys.* **561** (2014) A139 [[arXiv:1312.0777](#)] [[INSPIRE](#)].
- [53] D.A. Green, *A Revised Galactic Supernova Remnant Catalogue*, *Bull. Astron. Soc. India* **37** (2009) 45 [[arXiv:0905.3699](#)] [[INSPIRE](#)].
- [54] S.G. Lucek and A.R. Bell, *Non-linear amplification of a magnetic field driven by cosmic ray streaming*, *Mon. Not. Roy. Astron. Soc.* **314** (2000) 65.
- [55] J. Vink, J. Bleeker, K. Van Der Heyden, A. Bykov, A. Bamba et al., *The X-ray synchrotron emission of RCW 86 and the implications for its age*, *Astrophys. J.* **648** (2006) L33 [[astro-ph/0607307](#)] [[INSPIRE](#)].
- [56] LAT collaboration, A.A. Abdo et al., *Fermi LAT Observations of the Supernova Remnant W28 (G6.4-0.1)*, *Astrophys. J.* **718** (2010) 348 [[arXiv:1005.4474](#)] [[INSPIRE](#)].
- [57] A. Bell, K. Schure, B. Reville and G. Giacinti, *Cosmic ray acceleration and escape from supernova remnants*, *Mon. Not. Roy. Astron. Soc.* **431** (2013) 415 [[arXiv:1301.7264](#)] [[INSPIRE](#)].

- [58] K.M. Schure and A.R. Bell, *Cosmic ray acceleration in young supernova remnants*, *Mon. Not. Roy. Astron. Soc.* **435** (2013) 1174 [[arXiv:1307.6575](#)] [[INSPIRE](#)].
- [59] G. Morlino, E. Amato and P. Blasi, *Gamma ray emission from SNR RX J1713.7-3946 and the origin of galactic cosmic rays*, *Mon. Not. Roy. Astron. Soc.* **392** (2009) 240 [[arXiv:0810.0094](#)] [[INSPIRE](#)].
- [60] J.L. Han, W. Reich, X.H. Sun, X.Y. Gao, L. Xiao et al., *The sino-german $\Lambda 6$ cm polarization survey of the galactic plane: A summary*, *Int. J. Mod. Phys. Conf. Ser.* **23** (2013) 01110 [[arXiv:1202.1875](#)] [[INSPIRE](#)].
- [61] P. Madau, M. Della Valle and N. Panagia, *On the evolution of the cosmic supernova rates*, *Mon. Not. Roy. Astron. Soc.* **297** (1998) L17 [[astro-ph/9803284](#)] [[INSPIRE](#)].
- [62] R. Diehl, H. Halloin, K. Kretschmer, G.G. Lichti, V. Schoenfelder et al., *Radioactive Al-26 and massive stars in the galaxy*, *Nature* **439** (2006) 45 [[astro-ph/0601015](#)] [[INSPIRE](#)].
- [63] D.R. Lorimer, *The galactic population and birth rate of radio pulsars*, in *Young Neutron Stars and Their Environments*, F. Camilo and B.M. Gaensler eds., *IAU Symposium* **218** (2004) 105 [[astro-ph/0308501](#)] [[INSPIRE](#)].
- [64] D.H. Clark and J.L. Caswell, *A study of galactic supernova remnants, based on Molonglo-Parkes observational data*, *Mon. Not. Roy. Astron. Soc.* **174** (1976) 267.
- [65] P.F. Velazquez, G.M. Dubner, W.M. Goss and A.J. Green, *Investigation of the large scale neutral hydrogen near the supernova remnant W28*, *Astron. J.* **124** (2002) 2145 [[astro-ph/0207530](#)] [[INSPIRE](#)].
- [66] X.H. Sun, P. Reich, W. Reich, L. Xiao, X.Y. Gao et al., *A Sino-German 6cm polarization survey of the Galactic plane VII. Small supernova remnants*, *Astron. Astrophys.* **536** (2011) A83 [[arXiv:1110.1106](#)] [[INSPIRE](#)].
- [67] E. Furst, E. Hummel, W. Reich, Y. Sofue, W. Sieber et al., *A study of the composite supernova remnant G 18.95-1.1*, *Astron. Astrophys.* **209** (1989) 361.
- [68] E. Fuerst, W. Reich, and B. Aschenbach, *New radio and soft X-ray observations of the supernova remnant G 18.95-1.1.*, *Astron. Astrophys.* **319** (1997) 655.
- [69] I.M. Harrus, P.O. Slane, J.P. Hughes and P.P. Plucinsky, *An X-Ray study of the supernova remnant G18.95-1.1*, *Astrophys. J.* **603** (2004) 152 [[astro-ph/0311410](#)] [[INSPIRE](#)].
- [70] D. A. Green, *Sensitive OH observations towards 16 supernova remnants*, *Mon. Not. Roy. Astron. Soc.* **238** (1989) 737.
- [71] E.B. Giacani, G.M. Dubner, N.E. Kassim, D.A. Frail, W.M. Goss et al., *New Radio and Optical Study of the Supernova Remnant W44*, *Astron. J.* **113** (1997) 1379.
- [72] J.L. Caswell, J.D. Murray, R.S. Roger, D.J. Cole and D.J. Cooke, *Neutral hydrogen absorption measurements yielding kinematic distances for 42 continuum sources in the galactic plane*, *Astron. Astrophys.* **45** (1975) 239.
- [73] A. Wolszczan, J.M. Cordes, and R.J. Dewey, *Discovery of a young, 267 millisecond pulsar in the supernova remnant W44*, *Astrophys. J. Lett.* **372** (1991) L99.
- [74] J. Rho, R. Petre, E.M. Schlegel and J.J. Hester, *An X-ray and optical study of the supernova remnant W44*, *Astrophys. J.* **430** (1994) 757.
- [75] L. Xiao, W. Reich, E. Furst and J.L. Han, *Radio properties of the low surface brightness SNR G65.2+5.7*, *Astron. Astrophys.* **503** (2009) 827 [[arXiv:0904.3170](#)] [[INSPIRE](#)].
- [76] P.W. Gorham, P.S. Ray, S.B. Anderson, S.R. Kulkarni and T.A. Prince, *A Pulsar Survey of 18 Supernova Remnants*, *Astrophys. J.* **458** (1996) 257.
- [77] F. Mavromatakis, P. Boumis, J. Papamastorakis and J. Ventura, *Deep optical observations of g 65.3+5.7*, *Astron. Astrophys.* **388** (2002) 355 [[astro-ph/0204079](#)] [[INSPIRE](#)].

- [78] R. Kothes, T.L. Landecker and M. Wolleben, *H I Absorption of Polarized Emission: A New Technique for Determining Kinematic Distances to Galactic Supernova Remnants*, *Astrophys. J.* **607** (2004) 855.
- [79] R. Kothes, T.L. Landecker, W. Reich, S. Safi-Harb and Z. Arzoumanian, *DA495: an aging pulsar wind nebula*, *Astrophys. J.* **687** (2008) 516 [[arXiv:0807.0811](#)] [[INSPIRE](#)].
- [80] G. Castelletti, *A Multi-frequency study of the spectral index distribution in the SNR CTB 80*, *Astron. Astrophys.* **440** (2005) 171 [[astro-ph/0507716](#)] [[INSPIRE](#)].
- [81] R. Kothes, K. Fedotov, T. J. Foster and B. Uyaniker, *A catalogue of Galactic supernova remnants from the Canadian Galactic plane survey. I. Flux densities, spectra, and polarization characteristics*, *Astron. Astrophys.* **457** (2006) 1081.
- [82] R.G. Strom and B.W. Stappers, *Supernova Remnant CTB 80 and PSR 1951+32*, in *IAU Colloq. 177: Pulsar Astronomy - 2000 and Beyond*, M. Kramer, N. Wex and R. Wielebinski eds., *Astron. Soc. Pac. Conf. Ser.* **202** (2000) 509.
- [83] G. Castelletti, G. Dubner, K. Golap, W.M. Goss, P.F. Velazquez et al., *New high-resolution radio observations of the snr ctb 80*, *Astron. J.* **126** (2003) 2114 [[astro-ph/0310655](#)] [[INSPIRE](#)].
- [84] X. Sun, W. Reich, J.L. Han, P. Reich and R. Wielebinski, *New lambda-6cm observations of the cygnus loop*, *Astron. Astrophys.* (2005) [[astro-ph/0510509](#)] [[INSPIRE](#)].
- [85] W.P. Blair, R. Sankrit and J.C. Raymond, *Hubble Space Telescope Imaging of the Primary Shock Front in the Cygnus Loop Supernova Remnant*, *Astron. J.* **129** (2005) 2268.
- [86] W.P. Blair, R. Sankrit, S.I. Torres, P. Chayer and C.W. Danforth, *Far Ultraviolet Spectroscopic Explorer Observations of KPD 2055+3111, a Star behind the Cygnus Loop*, *Astrophys. J.* **692** (2009) 335.
- [87] Y. Ladouceur and S. Pineault, *New perspectives on the supernova remnant G78.2+2.1*, *Astron. Astrophys.* **490** (2008) 197.
- [88] A.M. Bykov, A.M. Krassilchtchikov, Y. Uvarov, H. Bloemen, R.A. Chevalier et al., *Hard x-ray emission clumps in the Gamma Cygni supernova remnant: An INTEGRAL-ISGRI view*, *Astron. Astrophys.* **427** (2004) L21 [[astro-ph/0410688](#)] [[INSPIRE](#)].
- [89] F. Mavromatakis, *Deep optical observations of the supernova remnant G 78.2+2.1*, *Astron. Astrophys.* **408** (2003) 237.
- [90] F. Mavromatakis, B. Aschenbach, P. Boumis and J. Papamastorakis, *Multi-wavelength study of the G 82.2+5.3 supernova remnant*, *Astron. Astrophys.* **415** (2004) 1051 [[astro-ph/0311530](#)] [[INSPIRE](#)].
- [91] M. Rosado and J. Gonzalez, *The Radial Velocity Field of the Optical Filaments Associated with the Supernova Remnant W63*, *Revista Mexicana de Astronomía y Astrofísica* **5** (1981) 93.
- [92] W. Reich, X. Zhang and E. Fürst, *35 cm observations of a sample of large supernova remnants*, *Astron. Astrophys.* **408** (2003) 961.
- [93] D.-Y. Byun, B.-C. Koo, K. Tatematsu and K. Sunada, *Interaction between the Supernova Remnant HB 21 and Molecular Clouds*, *Astrophys. J.* **637** (2006) 283.
- [94] J. Lazendic and P. Slane, *Enhanced abundances in three large-diameter mixed-morphology supernova remnants*, *Astrophys. J.* **647** (2006) 350 [[astro-ph/0505498](#)] [[INSPIRE](#)].
- [95] T.L. Landecker, D. Routledge, S.P. Reynolds, R.J. Smegal, K.J. Borkowski and F.D. Seward, *DA 530: A Supernova Remnant in a Stellar Wind Bubble*, *Astrophys. J.* **527** (1999) 866.
- [96] T. Foster and D. Routledge, *A New Distance Technique for Galactic Plane Objects*, *Astrophys. J.* **598** (2003) 1005.

- [97] B. Uyaniker, R. Kothes and C.M. Brunt, *The supernova remnant ctb104a : magnetic field structure and interaction with the environment*, *Astrophys. J.* **565** (2002) 1022 [[astro-ph/0110001](#)] [[INSPIRE](#)].
- [98] F. Mantovani, M. Nanni, C.J. Salter and P. Tomasi, *Further observations of radio sources from the BG survey. I - The non-thermal sources near L equals 94 deg*, *Astron. Astrophys.* **105** (1982) 176.
- [99] R. Kothes, B. Uyaniker and A. Yar, *The distance to the snr ctb109 deduced from its environment*, *Astrophys. J.* **576** (2002) 169 [[astro-ph/0205034](#)] [[INSPIRE](#)].
- [100] A.N. Parmar, T. Oosterbroek, F. Favata, S. Pightling, M.J. Coe et al., *A BeppoSAX observation of the X-ray pulsar 1E2259+586hfill and the supernova remnant (CTB109)*, *Astron. Astrophys.* **330** (1998) 175 [[astro-ph/9709248](#)] [[INSPIRE](#)].
- [101] V.A. Hughes, R.H. Harten and S. van den Bergh, *A new supernova remnant G109.2-1.0*, *Astrophys. J. Lett.* **246** (1981) L127.
- [102] R. Kothes, B. Uyaniker and R.I. Reid, *Two new Perseus arm supernova remnants discovered in the Canadian Galactic Plane Survey*, *Astron. Astrophys.* **444** (2005) 871.
- [103] A. Yar-Uyaniker, B. Uyaniker and R. Kothes, *Distance of three supernova remnants from HI line observations in a complex region: G114.3+0.3, G116.5+1.1 and CTB 1 (G116.9+0.2)*, *Astrophys. J.* **616** (2004) 247 [[astro-ph/0408386](#)] [[INSPIRE](#)].
- [104] S. Pineault, T.L. Landecker, C.M. Swerdlyk and W. Reich, *The supernova remnant CTA1 (G 119.5+10.3): a study. of the breakout phenomenon*, *Astron. Astrophys.* **324** (1997) 1152.
- [105] S. Pineault, T.L. Landecker, B. Madore and S. Gaumont-Guay, *The supernova remnant CTA1 and the surrounding interstellar medium*, *Astron. J.* **105** (1993) 1060.
- [106] D.A. Leahy and W.-W. Tian, *Radio observations and spectrum of the snr g127.1+0.5 and its central source 0125+628*, *Astron. Astrophys.* **451** (2006) 251 [[astro-ph/0601487](#)] [[INSPIRE](#)].
- [107] G. Joncas, R.S. Roger and P.E. Dewdney, *New radio observations of two supernova remnants in Cassiopeia - G126.2+1.6 and G127.1+0.5*, *Astron. Astrophys.* **219** (1989) 303.
- [108] R. Fesen, G. Rudie, A. Hurford and A. Soto, *Optical Imaging and Spectroscopy of the Galactic Supernova Remnant 3C 58 (G130.7+3.1)*, *Astrophys. J. Suppl.* **174** (2008) 379.
- [109] Y. Shibanov, N. Lundqvist, P. Lundqvist, J. Sollerman and D. Zyuzin, *Optical identification of the 3C 58 pulsar wind nebula*, *Astron. Astrophys.* **486** (2008) 273 [[arXiv:0802.2386](#)] [[INSPIRE](#)].
- [110] W.B. Shi, J.L. Han, X.Y. Gao, X.H. Sun, L. Xiao et al., *The radio spectrum and magnetic field structure of SNR HB3*, *Astron. Astrophys.* **487** (2008) 601 [[arXiv:0806.1647](#)] [[INSPIRE](#)].
- [111] Y. Xu, M.J. Reid, X.W. Zheng and K.M. Menten, *The distance to the perseus spiral arm in the milky way*, *Science* **311** (2006) 54 [[astro-ph/0512223](#)] [[INSPIRE](#)].
- [112] W. Reich, E. Fuerst and E.M. Arnal, *Radio observations of the bright X-ray supernova remnant G156.2+5.7*, *Astron. Astrophys.* **256** (1992) 214.
- [113] S. Katsuda, R. Petre, U. Hwang, H. Yamaguchi, K. Mori et al., *Suzaku Observations of Thermal and Non-Thermal X-Ray Emission from the Middle-Aged Supernova Remnant G156.2+5.7*, *Publ. Astron. Soc. Jap.* **61** (2009) S155 [[arXiv:0902.1782](#)] [[INSPIRE](#)].
- [114] J.W. Xu, J.L. Han, X.H. Sun, W. Reich, L. Xiao et al., *Polarization observations of SNR G156.2+5.7 at λ 6cm*, *Astron. Astrophys.* **470** (2007) 969 [[arXiv:0705.2806](#)] [[INSPIRE](#)].
- [115] S. Yamauchi, K. Koyama, H. Tomida, J. Yokogawa and K. Tamura, *ASCA Observations of the Supernova Remnant G156.2+5.7*, *Pub. Astron. Soc. Japan* **51** (1999) 13.
- [116] D.A. Leahy and W. Tian, *Radio Spectrum and Distance of the SNR HB9*, *Astron. Astrophys.* **461** (2007) 1013 [[astro-ph/0606598](#)] [[INSPIRE](#)].

- [117] L. Xiao, E. Furst, W. Reich and J.L. Han, *Radio spectral properties and the magnetic field of the SNR S147*, *Astron. Astrophys.* **482** (2008) 783 [[arXiv:0801.4803](#)] [[INSPIRE](#)].
- [118] S.B. Anderson, B.J. Cadwell, B.A. Jacoby, A. Wolszczan, R.S. Foster and M. Kramer, *A 143 Millisecond Radio Pulsar in the Supernova Remnant S147*, *Astrophys. J. Lett.* **468** (1996) L55.
- [119] C.-Y. Ng, R.W. Romani, W.F. Brisken, S. Chatterjee and . Kramer, Michael, *The Origin and Motion of PSR J0538+2817 in S147*, *Astrophys. J.* **654** (2006) 487 [[astro-ph/0611068](#)] [[INSPIRE](#)].
- [120] . Kramer, Michael, A.G. Lyne, G. Hobbs, O. Lohmer, P. Carr et al., *Proper motion, age and initial spin period of PSR J0538+2817 in S147*, *Astrophys. J.* **593** (2003) L31 [[astro-ph/0306628](#)] [[INSPIRE](#)].
- [121] H.E.S.S. collaboration, F. Aharonian et al., *Observations of the Crab Nebula with H.E.S.S.*, *Astron. Astrophys.* **457** (2006) 899 [[astro-ph/0607333](#)] [[INSPIRE](#)].
- [122] B.Y. Welsh and S. Sallmen, *High-velocity NaI and CaII absorption components observed towards the IC 443 SNR*, *Astron. Astrophys.* **408** (2003) 545.
- [123] J.-J. Lee, B.-C. Koo, M.S. Yun, S. Stanimirović, C. Heiles and M. Heyer, *A 21 cm Spectral and Continuum Study of IC 443 Using the Very Large Array and the Arecibo Telescope*, *Astron. J.* **135** (2008) 796.
- [124] D.A. Graham, C.G. T. Haslam, C.J. Salter and W.E. Wilson, *A continuum study of galactic radio sources in the constellation of Monoceros*, *Astron. Astrophys.* **109** (1982) 145.
- [125] V.B. Jovanovic and D. Urosevic, *The Monoceros radio loop: temperature, brightness, spectral index and distance*, *Astronomische Nachrichten* **330** (2009) 741 [[arXiv:0904.2261](#)] [[INSPIRE](#)].
- [126] C. Bonatto and E. Bica, *Probing the age and structure of the nearby very young open clusters NGC 2244 and NGC 2239*, *Mon. Not. Roy. Astron. Soc.* **394** (2009) 2127 [[arXiv:0901.0833](#)] [[INSPIRE](#)].
- [127] B.Y. Welsh, D.M. Sfeir, S. Sallmen and R. Lallement, *Far Ultraviolet Spectroscopic Explorer observations of high-velocity gas associated with the Monoceros Loop SNR*, *Astron. Astrophys.* **372** (2001) 516.
- [128] G. Castelletti, G. Dubner, K. Golap and W.M. Goss, *New VLA observations of the SNR Puppis A: The radio properties and the correlation with the X-ray emission*, *Astron. Astrophys.* **459** (2006) 535 [[astro-ph/0607200](#)] [[INSPIRE](#)].
- [129] G.M. Dubner and E.M. Arnal, *Neutral hydrogen and carbon monoxide observations towards the SNR Puppis A*, *Astron. Astrophys.s* **75** (1988) 363.
- [130] E.M. Reynoso, G.M. Dubner, W.M. Goss and E.M. Arnal, *VLA Observations of Neutral Hydrogen in the Direction of Puppis A*, *Astron. J.* **110** (1995) 318.
- [131] P.F. Winkler, J.H. Tuttle, R.P. Kirshner and M.J. Irwin, *Kinematics of Oxygen-Rich Filaments in Puppis a*, in *IAU Colloq. 101: Supernova Remnants and the Interstellar Medium*, R.S. Roger and T.L. Landecker eds. (1988) pg. 65.
- [132] H. Alvarez, J. Aparici, J. May and P. Reich, *The radio spectral index of the Vela supernova remnant*, *Astron. Astrophys.* **372** (2001) 636.
- [133] A.N. Cha, K.R. Sembach and A.C. Danks, *The distance to the vela supernova remnant*, *Astrophys. J. Lett.* **515** (1999) L25 [[astro-ph/9902230](#)] [[INSPIRE](#)].
- [134] P.A. Caraveo, A. De Luca, R.P. Mignani and G.F. Bignami, *The distance to the vela pulsar gauged with HST parallax observations*, *Astrophys. J.* **561** (2001) 930 [[astro-ph/0107282](#)] [[INSPIRE](#)].
- [135] J.H. Taylor, R.N. Manchester and A.G. Lyne, *Catalog of 558 pulsars*, *Astrophys. J. Suppl.* **88** (1993) 529 [[INSPIRE](#)].

- [136] M. Miceli, F. Bocchino and F. Reale, *Physical and chemical inhomogeneities inside the Vela SNR shell. Indications of ejecta shrapnels*, *Astrophys. J.* **676** (2008) 1064 [[arXiv:0712.3017](#)] [[INSPIRE](#)].
- [137] S. Katsuda, H. Tsunemi and K. Mori, *The Slow X-Ray Expansion of the Northwestern Rim of the Supernova Remnant RX J0852.0-4622*, *Astrophys. J. Lett.* **678** (2008) L35 [[arXiv:0803.3266](#)] [[INSPIRE](#)].
- [138] M.P. Redman and J. Meaburn, *A possible association of a young pulsar (PSR J0855-4644) with the young Vela supernova remnant RX J0852.0-4622*, *Mon. Not. Roy. Astron. Soc.* **356** (2005) 969.
- [139] B. Aschenbach, *Discovery of a young nearby supernova remnant*, *Nature* **396** (1998) 141.
- [140] A.F. Iyudin, V. Schönfelder, K. Bennett, H. Bloemen, R. Diehl et al., *Emission from ^{44}Ti associated with a previously unknown Galactic supernova*, *Nature* **396** (1998) 142.
- [141] A.R. Duncan, R.T. Stewart, R.F. Haynes and K.L. Jones, *Supernova remnant candidates from the Parkes 2.4-GHz survey*, *Mon. Not. Roy. Astron. Soc.* **287** (1997) 722.
- [142] M. Stupar, Q.A. Parker and M.D. Filipovic, *G315.1+2.7: A new Galactic SNR from the AAO/UKST H α survey*, *Mon. Not. Roy. Astron. Soc.* **374** (2007) 1441 [[astro-ph/0612771](#)] [[INSPIRE](#)].
- [143] J.R. Dickel, R.G. Strom and D.K. Milne, *The radio structure of the supernova remnant msh14-63*, *Astrophys. J.* **546** (2001) 447 [[astro-ph/0008042](#)] [[INSPIRE](#)].
- [144] M. Rosado, P. Ambrocio-Cruz, E. Le Coarer and M. Marcelin, *Kinematics of the galactic supernova remnants RCW 86, MSH 15-56 and MSH 11-61A.*, *Astron. Astrophys.* **315** (1996) 243.
- [145] J. Sollerman, P. Ghavamian, P. Lundqvist and R.C. Smith, *High resolution spectroscopy of Balmer-dominated shocks in the RCW 86, kepler and sn 1006 supernova remnants*, *Astron. Astrophys.* **407** (2003) 249 [[astro-ph/0306196](#)] [[INSPIRE](#)].
- [146] R.S. Roger, D.K. Milne, M.J. Kesteven, K.J. Wellington and R.F. Haynes, *Symmetry of the radio emission from two high-latitude supernova remnants, G296.5+10.0 and G327.6+14.6 (1006)*, *Astrophys. J.* **332** (1988) 940.
- [147] E. Kalemci, S.E. Boggs, P.A. Milne and S.P. Reynolds, *Searching for annihilation radiation from sn 1006 with spi on integral*, *Astrophys. J.* **640** (2006) L55 [[astro-ph/0602233](#)] [[INSPIRE](#)].
- [148] P.F. Winkler, G. Gupta and K.S. Long, *The SN 1006 remnant: Optical proper motions, deep imaging, distance and brightness at maximum*, *Astrophys. J.* **585** (2003) 324 [[astro-ph/0208415](#)] [[INSPIRE](#)].
- [149] A. Bamba, Y. Fukazawa, J.S. Hiraga, J.P. Hughes, H. Katagiri et al., *Suzaku wide-band observations of SN 1006*, *Pub. Astron. Soc. Japan* **60** (2008) 153 [[arXiv:0708.0073](#)] [[INSPIRE](#)].
- [150] D.A. Leahy, J. Nousek and A.J. S. Hamilton, *HEAO 1 A-2 low-energy detector X-ray spectra of the Lupus Loop and SN 1006*, *Astrophys. J.* **374** (1991) 218.
- [151] J.-H. Shinn, K.W. Min, C.-N. Lee, J. Edelstein, E.J. Korpela et al., *Diffuse Far-ultraviolet Observation of the Lupus Loop Region*, *Astrophys. J.* **644** (2006) L189 [[astro-ph/0604454](#)] [[INSPIRE](#)].
- [152] J.S. Lazendic, P.O. Slane, B.M. Gaensler, S.P. Reynolds, P.P. Plucinsky et al., *A High - resolution study of nonthermal radio and x-ray emission from SNR G347.3-0.5*, *Astrophys. J.* **602** (2004) 271 [[astro-ph/0310696](#)] [[INSPIRE](#)].

- [153] C.S. Shen, *Pulsars and Very High-Energy Cosmic-Ray Electrons*, *Astrophys. J. Lett.* **162** (1970) L181.
- [154] A.K. Harding and R. Ramaty, *The Pulsar Contribution to Galactic Cosmic Ray Positrons*, *Int. Cos. Ray Conf.* **2** (1987) 92.
- [155] J. Arons, *Pulsars as Gamma-Rays Sources: Nebular Shocks and Magnetospheric Gaps*, *Space Sci. Rev.* **75** (1996) 235.
- [156] L. Zhang and K.S. Cheng, *Cosmic-ray positrons from mature gamma-ray pulsars*, *Astron. Astrophys.* **368** (2001) 1063.
- [157] E. Amato, *The theory of pulsar wind nebulae*, [[arXiv:1312.5945](#)] [[INSPIRE](#)].
- [158] M. Ruderman and P. Sutherland, *Theory of pulsars: Polar caps, sparks and coherent microwave radiation*, *Astron. J.* **196** (1975) 51.
- [159] A. Cheng, M. Ruderman and P. Sutherland, *Current flow in pulsar magnetospheres*, *Astrophys. J.* **203** (1976) 209.
- [160] K. Cheng, C. Ho and M.A. Ruderman, *Energetic Radiation from Rapidly Spinning Pulsars. 1. Outer Magnetosphere Gaps. 2. Vela and Crab*, *Astron. J.* **300** (1986) 500.
- [161] M.J. Rees and J.E. Gunn, *The origin of the magnetic field and relativistic particles in the Crab Nebula*, *Mon. Not. Roy. Astron. Soc.* **167** (1974) 1 [[INSPIRE](#)].
- [162] FERMI-LAT collaboration, D. Grasso et al., *On possible interpretations of the high energy electron-positron spectrum measured by the Fermi Large Area Telescope*, *Astropart. Phys.* **32** (2009) 140 [[arXiv:0905.0636](#)] [[INSPIRE](#)].
- [163] A.M. Atoyan and F.A. Aharonian, *On the mechanisms of gamma radiation in the Crab Nebula*, *Mon. Not. Roy. Astron. Soc.* **278** (1996) 525.
- [164] D. Malyshev, I. Cholis and J. Gelfand, *Pulsars versus Dark Matter Interpretation of ATIC/PAMELA*, *Phys. Rev. D* **80** (2009) 063005 [[arXiv:0903.1310](#)] [[INSPIRE](#)].
- [165] H.E.S.S. collaboration, F. Aharonian et al., *First detection of a VHE gamma-ray spectral maximum from a cosmic source: HESS discovery of the Vela X nebula*, *Astron. Astrophys.* **448** (2006) L43 [[astro-ph/0601575](#)] [[INSPIRE](#)].
- [166] A.M. Atoyan and F.A. Aharonian, *On the mechanisms of gamma radiation in the crab nebula*, *Mon. Not. Roy. Astron. Soc.* **278** (1996) 525.
- [167] THE FERMI-LAT collaboration, A.A. Abdo et al., *The Second Fermi Large Area Telescope Catalog of Gamma-ray Pulsars*, *Astrophys. J. Suppl.* **208** (2013) 17 [[arXiv:1305.4385](#)] [[INSPIRE](#)].
- [168] P. Blasi and E. Amato, *Positrons from pulsar winds*, [[arXiv:1007.4745](#)] [[INSPIRE](#)].
- [169] AMS-02 collaboration, H. Haino, *Precision measurement of the proton flux with AMS*, talk at *33rd ICRC Conference* (2013).
- [170] AMS-02 collaboration, V. Choutko, *Precision measurement of the helium flux with AMS*, talk at *33rd ICRC Conference* (2013).
- [171] T. Kamae, N. Karlsson, T. Mizuno, T. Abe and T. Koi, *Parameterization of Gamma, e^\pm and Neutrino Spectra Produced by p - p Interaction in Astronomical Environment*, *Astrophys. J.* **647** (2006) 692 [*Erratum ibid.* **662** (2007) 779] [[astro-ph/0605581](#)] [[INSPIRE](#)].
- [172] C.D. Dermer, J.D. Finke, R.J. Murphy, A.W. Strong, F. Loparco et al., *On the Physics Connecting Cosmic Rays and Gamma Rays: Towards Determining the Interstellar Cosmic Ray Spectrum*, [[arXiv:1303.6482](#)] [[INSPIRE](#)].

- [173] COLLABORATION FOR THE FERMI collaboration, C.D. Dermer, A.W. Strong, E. Orlando and L. Tibaldo, *Determining the Spectrum of Cosmic Rays in Interstellar Space from the Diffuse Galactic Gamma-Ray Emissivity*, [arXiv:1307.0497](#) [INSPIRE].
- [174] D. Maurin, F. Donato, R. Taillet and P. Salati, *Cosmic rays below $z=30$ in a diffusion model: new constraints on propagation parameters*, *Astrophys. J.* **555** (2001) 585 [[astro-ph/0101231](#)] [INSPIRE].
- [175] F. Donato, N. Fornengo, D. Maurin and P. Salati, *Antiprotons in cosmic rays from neutralino annihilation*, *Phys. Rev. D* **69** (2004) 063501 [[astro-ph/0306207](#)] [INSPIRE].
- [176] L.A. Fisk, *Solar modulation of galactic cosmic rays, 2*, *J. Geophys. Res.* **76** (1971) 221.
- [177] J.S. Perko, *Solar modulation of galactic antiprotons*, *Astron. Astrophys.* **184** (1987) 119.
- [178] L. Maccione, *Low energy cosmic ray positron fraction explained by charge-sign dependent solar modulation*, *Phys. Rev. Lett.* **110** (2013) 081101 [[arXiv:1211.6905](#)] [INSPIRE].
- [179] S. Della Torre, P. Bobik, M.J. Boschini, C. Consolandi, M. Gervasi et al., *Effects of solar modulation on the cosmic ray positron fraction*, *Adv. Space Res.* **49** (2012) 1587.
- [180] A.W. Strong, E. Orlando and T.R. Jaffe, *The interstellar cosmic-ray electron spectrum from synchrotron radiation and direct measurements*, *Astron. Astrophys.* **534** (2011) A54 [[arXiv:1108.4822](#)] [INSPIRE].
- [181] E. Orlando and A. Strong, *Galactic synchrotron emission with cosmic ray propagation models*, *Mon. Not. Roy. Astron. Soc.* **436** (2013) 2127 [[arXiv:1309.2947](#)] [INSPIRE].
- [182] J.J. Beatty, A. Bhattacharyya, C. Bower, S. Coutu, M.A. DuVernois et al., *New measurement of the cosmic-ray positron fraction from 5 to 15-GeV*, *Phys. Rev. Lett.* **93** (2004) 241102 [[astro-ph/0412230](#)] [INSPIRE].
- [183] S.W. Barwick, J.J. Beatty, C.R. Bower, C.J. Chaput, S. Coutu et al., *The Energy spectra and relative abundances of electrons and positrons in the galactic cosmic radiation*, *Astrophys. J.* **498** (1998) 779 [[astro-ph/9712324](#)] [INSPIRE].
- [184] HEAT collaboration, S.W. Barwick et al., *Measurements of the cosmic ray positron fraction from 1-GeV to 50-GeV*, *Astrophys. J.* **482** (1997) L191 [[astro-ph/9703192](#)] [INSPIRE].
- [185] M.A. DuVernois, S.W. Barwick, J.J. Beatty, A. Bhattacharyya, C.R. Bower et al., *Cosmic ray electrons and positrons from 1-GeV to 100-GeV: Measurements with HEAT and their interpretation*, *Astrophys. J.* **559** (2001) 296 [INSPIRE].
- [186] M. Boezio, P. Carlson, T. Francke, N. Weber, M. Suffert et al., *The Cosmic-Ray Electron and Positron Spectra Measured at 1 AU during Solar Minimum Activity*, *Astrophys. J.* **532** (2000) 653 [INSPIRE].
- [187] M. Boezio, G. Barbiellini, et al., *Measurements of cosmic-ray electrons and positrons by the Wizard/CAPRICE collaboration*, *Adv. Space Res.* **27** (2001) 669.
- [188] K. Yoshida, S. Torii, T. Yamagami, et al., *Cosmic-ray electron spectrum above 100 GeV from PPB-BETS experiment in Antarctica*, *Adv. Space Res.* **42** (2008) 1670.
- [189] S. Torii, T. Tamura, N. Tateyama, K. Yoshida, J. Nishimura et al., *The energy spectrum of cosmic ray electrons from 10-GeV to 100-GeV observed with a highly granulated imaging calorimeter*, *Astrophys. J.* **559** (2001) 973 [INSPIRE].
- [190] H.E.S.S. collaboration, F. Aharonian et al., *Probing the ATIC peak in the cosmic-ray electron spectrum with H.E.S.S.*, *Astron. Astrophys.* **508** (2009) 561 [[arXiv:0905.0105](#)] [INSPIRE].
- [191] I.G. Usoskin, K. Alanko-Huotari, G.A. Kovaltsov and K. Mursula, *Heliospheric modulation of cosmic rays: Monthly reconstruction for 1951-2004*, *J. Geophys. Res. (Space Phys.)* **110** (2005) 12108.

- [192] I.G. Usoskin, G.A. Bazilevskaya and G.A. Kovaltsov, *Solar modulation parameter for cosmic rays since 1936 reconstructed from ground-based neutron monitors and ionization chambers*, *J. Geophys. Res. (Space Phys.)* **116** (2011) 2104.
- [193] H. Yuksel, M.D. Kistler and T. Stanev, *TeV Gamma Rays from Geminga and the Origin of the GeV Positron Excess*, *Phys. Rev. Lett.* **103** (2009) 051101 [[arXiv:0810.2784](#)] [[INSPIRE](#)].
- [194] I. Cholis and D. Hooper, *Dark Matter and Pulsar Origins of the Rising Cosmic Ray Positron Fraction in Light of New Data From AMS*, *Phys. Rev. D* **88** (2013) 023013 [[arXiv:1304.1840](#)] [[INSPIRE](#)].